INVESTIGATING THE EFFECTS OF PULSED RADIOFREQUENCY THERAPY IN THE BLOCKING OF ACTION POTENTIALS IN NERVES

by

Aryan Safakish

B.Sc., Ryerson University, Toronto, 2017

A thesis

presented to Ryerson University

in partial fulfillment of the

requirements for the degree of

Master of Science

in the program of

Biomedical Physics

Toronto, Ontario, Canada, 2020

Author's Declaration

I hereby declare that I am the sole author of this thesis. This is a true copy of the thesis, including any required final revisions, as accepted by my examiners.

I authorize Ryerson University to lend this thesis to other institutions or individuals for the purpose of scholarly research.

I further authorize Ryerson University to reproduce this thesis by photocopying or by other means, in total or in part, at the request of other institutions or individuals for the purpose of scholarly research.

I understand that my thesis may be made electronically available to the public.

Aryan Safakish.

Investigating the Effects of Pulsed Radiofrequency Therapy in The Blocking of Action Potentials in Nerves, Aryan Safakish, Master of Science, Biomedical Physics, Ryerson University, 2020

Abstract

Radiofrequency (RF) currents (pulsed or continuous mode) are used as a treatment modality for chronic pain management. This is achieved by blocking sensory nerves' ability to propagate pain signals. In this thesis, it was proposed that pulsed RF (PRF) therapy can block action potential propagation, and that when used in clinical settings, deliver thermal doses below the threshold for thermal damage to nerves. A neurophysiology system with stimulating and reading electrodes was used to study earthworm nerves before and after PRF therapy. It was shown that 60% of earthworms in the high-voltage-group treated with bipolar PRF experienced a block in action potential propagation. Computer simulations of the electrical field and heating patterns were created, experimentally validated, and after determining a threshold thermal dose for nerve damage, it was shown that for C6 medial branch nerve PRF therapy the temperature at the nerve was not high enough to cause thermal damage.

Acknowledgements

First and foremost, I would like to express my gratitude to Dr. Carl Kumaradas for teaching me so much in the last two years. From learning about the physics of RF therapy and computational modeling, to adjustments that a recent undergrad student needs to make to become a successful graduate student. I couldn't have asked for a better supervisor. Next I would also like to thank Dr. Hisham Assi for his ever-present support with COMSOL. Additionally, I would like to thank the members of my supervisory committee, Dr. Jahan Tavakkoli and Dr. Michael C. Kolios for their time and helpful comments. I would also like to show my appreciation to Dr. Graham Ferrier for his technical help in the experimental design.

I must express my profound gratitude to my family for providing me with unfailing support and encouragement throughout my years of study and teaching me to think scientifically. Finally, I have to thank my fiancé Erica Greco. Living with you and being able to call you my partner for life is truly a pleasure and drives me to push through in the toughest moments. Thank you.

Table of Contents

List of Tables

List of Figures

1 Introduction

Pain is highly individual and subjective from one person to another, thus defining and treating it can be quite challenging.[1] Chronic, or persistent pain, can be experienced in response to an initial injury, or even in certain cases, in the absence of any past injury.[2] The symptoms of chronic pain vary widely due to a myriad of factors, but some common symptoms include headaches, lower back pain, neurogenic pain (resulting from damaged peripheral nerves or to the central nervous system), or psychogenic pain (pain not due to any known injury).[2]

Risk of experiencing pain increases with age and according to Statistics Canada, in 2014 approximately 6 million individuals or 15.6% of Canadians were aged 65 years or older.[3] Models predict that by the year 2030, there will be a total of 9 million individuals aged 65 or older, making up 23% of the country's population.[3] With an aging population, considerable attention should be given to the rising cost of health care.

Chronic pain (CP), like many other ailments, is not only a cost to the health care system but contributes to a reduction in productivity. Often, those suffering symptoms of chronic pain are limited both physically and emotionally. It has been estimated that in Canada, with more than $6 billion per year in direct health care cost and $37 billion per year in lost productivity, chronic pain costs outweigh those of cancer, heart disease and HIV combined. [4]

Breivik, Collett, Ventafridda et al., (2006) used a questionnaire to determine the prevalence of CP in Europe. Respondents were considered to experience 'chronic pain' if they (i) had suffered from pain for at least six months, (ii) had experienced pain in the last month, (iii) experienced pain at least two times per week and (iv) rated their pain intensity when they last experienced pain as

at least 5 on a 10-point numerical rating scale, where 1 = no pain at all and 10 = the worst pain imaginable.[5]

According to a survey conducted on a representative sample of the Canadian population in 2007, 44.4% of Canadians consider themselves to be suffering from pain and 19% of those surveyed suffered from CP (as defined by the criteria set by Breivik et al., 2006).[6]

1.1 Chronic Pain Management

There are countless approaches to managing or alleviating the symptoms of chronic pain for patients. These interventions include medical, physical, psychological, or some combination of treatments. Most patients will often try multiple treatments to find one that works best for their individual case.[7]

1.1.1 Psychological and Physical Therapy

To alleviate the symptoms of CP, patients have many options that help with varying degrees of effectiveness. For patients interested in non-medicinal treatments, options worth exploring include physical therapy and rehabilitation, exercise, acupuncture, massage, yoga, chiropractic care, and many more.[7] Alternatively, common psychological chronic pain management techniques include – but are not limited to – CBT, stress reduction, meditation, and hypnosis.[7]

1.1.2 Medicinal Approach

Various medications can assist in alleviating the symptoms of CP to varying degrees. Some of these medications are administered orally, and others administered by injections near the site of injury. Furthermore, there are some procedural approaches as well which will be covered in the subsections to come.

1.1.2.1 Oral Medication Approach

Pain medications function in various ways by targeting mostly the neuronal synapses, and the regular functioning of neurotransmitters (discussed later). Some examples include serotonin/norepinephrine reuptake inhibitors (duloxetine and benlafexine), nonsteroidal anti-inflammatory drugs (celecoxib, ibuprofen, aspirin), muscle relaxants like baclofen, opioids (hydrocodone, oxycodone, hydromorphone, fentanyl), and cannabinoids. With the exception of some nonsteroidal anti-inflammatory drugs, the majority orally administered medication for CP management should be prescribed by a physician.[7]

Of the previously mentioned examples, one of the most popular is the use of 'pain killers' or Opioids. In 2015, 1 in 133 deaths in Ontario (Canada's most populous province) were opioid related.[8] Patrick Fitch, the President and Internal Liason for the Canadian Society of Hospital Pharmacists refers to Canada as being "in the midst of an opioid crisis".[9] Fitch cites more than 2900 opioid-related deaths having occurred in 2016, and nearly 3000 in just the first seven months of 2017.[9] In September of 2019, Purdue Pharma LP, the producers of the highly addictive OxyContin had to file for bankruptcy, after it was proven in court that they created a public nuisance with their mishandling of the medicines.[10] These mishandlings included illegally marketing the painkiller failing to oversee orders, and ignoring red flags in regards to unusually frequent prescriptions.[10]

It is worth noting that THC/CBD (tetrahydrocannabinol/cannabidiol) oral sprays have shown promise, particularly in otherwise treatment-resistant patients, in alleviating pain symptoms.[11] With the recent federal legalization of Cannabis in Canada, it is expected that the future of research in this field will become more substantial, as well as offer an alternative to Opioids.

1.1.2.2 Minimally Invasive Procedures

Other approaches to CP management include medical injections. For example, trigger point injections involves injection of fluid into the trigger point.[12] The trigger point is defined as hyperirritable areas (2-5 mm diameter) of tissue that are tender when compressed and give rise to the patient's pain.[12] There have been a variety of trigger point injection fluids including water, saline, vitamin B solutions, and corticosteroids.[12] Tissue irritation caused by the injection can be reduced by including local anesthetics (procaine, lidocaine, bupivacaine, etc) into the injection fluid.[12]

In addition to trigger point injections, epidural injections have also shown promise in alleviating the symptoms of CP. In one study, morphine (opiate) and bupivacaine (anesthetic) proved to be an effective combination for epidural injections to treat lumbosacral radicular CP.[13] Guided with fluoroscopy, an epidural catheter was inserted into the T12-L1 intervertebral space and the patient was injected three times per day for 30 days before the catheter was removed.[13] This method showed at least a 30% reduction in a self-reported 1-10 numerical rating scale (1 = no pain, 10 = unbearable pain) in 73% of the patients involved.[13] Similarly, other epidural injections could substitute the opiate with a corticosteroid, thereby focusing on the inflammatory pathway.[14]

One non-invasive treatment worth noting is the application of magnetic resonance imaging guided high-intensity focused ultrasound (MR-HIFU) to target the nerve by creating heating a small volume of tissue to a desired temperature.[15] MR-HIFU applications have shown effective in treating sacroiliac joint (SIJ) pain for up to 6 months.[15] While this technique shows promise, it requires MR imaging, which is costly, particularly in comparison to the fluoroscopy/CT guided imaging typically used in other treatment modalities.

1.1.3 Radiofrequency Therapy

Radiofrequency ablation is one of the treatment options that is available to CP patients and is the focus of this thesis. This treatment is carried out by clinicians (anesthesiologists) under the guidance of radiological imaging. The anesthesiologist will target particular sensory nerve(s) which he/she believes are the source of a patient's chronic pain. As shown in Figure 1, an insulated RF electrode with an uninsulated active tip is placed in that target region with the aim of blocking the nerve's ability to conduct pain signals to the brain.

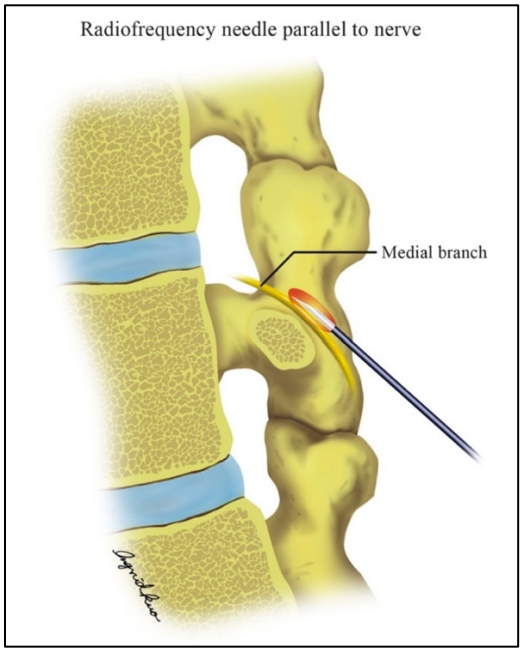

Figure 1 – Typical location of monopolar RF needle for medial branch nerve lesioning. [16]

1.2 The Nervous System

Of all the various bodily systems (reproductive system, digestive system, etc), the nervous system is perhaps the most complex, both in terms of our understanding and its functions. The nervous system plays a necessary role in the normal functioning of the human body with responsibilities including, but not limited to, maintaining homeostasis, receiving sensory input, integrating information, controlling muscles and glands, and establishing and maintaining mental activity.[17] To understand the pain pathway, it's important to focus on the structures responsible for the transmission of pain signals as well as how those pain signals are created.

1.2.1 What Is Pain?

In response to an injury, our body perceives pain as a sort of alarm that something is not right. For example, an athlete who sprains an ankle will feel acute pain in the ankle region, often coupled with swelling, and even bruising. These bodily responses (particularly the extreme pain) make putting weight on the injured ankle quite challenging. The athlete copes with this pain by using a crutch or a walking boot, and thereby promote healing by reducing the load on the impacted area. Pain signals (action potentials) are transmitted from the site of injury to the spinal cord, which are then transmitted from the spinal cord to the brain where pain is perceived. The transmissions are carried by sensory neurons in the afferent pathway, seen in Figure 2. Sensory neurons specific to pain are referred to as *nociceptors.*[17] Most sensory receptors are responsive to one type of stimuli, but nociceptors are distributed throughout the body and respond to extreme mechanical, chemical, or thermal stimuli.[17]

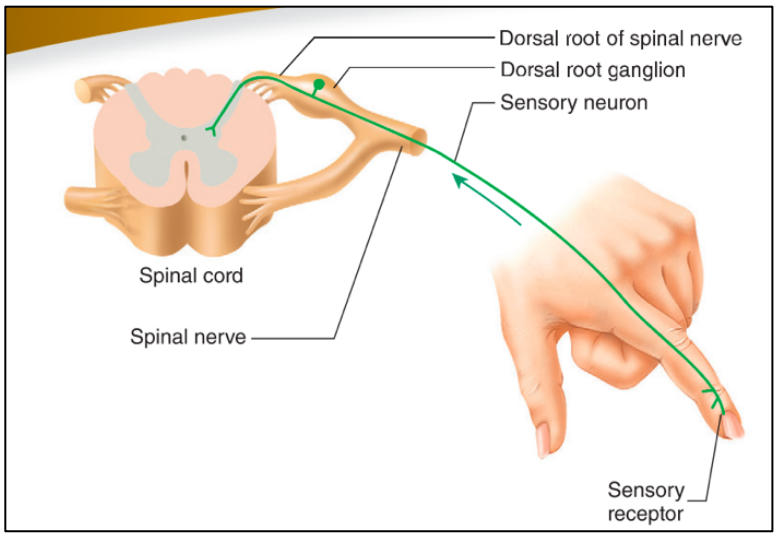

Figure 2 - Sensory (afferent) pathway. The dorsal root ganglion is a common source of chronic pain.[17]

The level of pain one feels depends on the intensity, quality, and duration of the stimuli, which is why a scratch and a cut have distinguishably different levels of pain.[18]

1.2.2 Action Potentials

Nerves transmit action potentials through a very interesting electrochemical chain of events. In order to understand this process, it is important to consider the anatomy and physiology of a typical neuron (which make up nerves). Neurons, similar to most other cells in the human body, encompass various organelles with specific roles vital to the functioning of the cell, which can be seen in Figure 3. Organelles like the nucleus, mitochondrion, and Golgi apparatus are fundamental, and found in almost all cells. Neurons are interesting in that they contain finger-like structures called axons and dendrites. The nervous system is responsible for all of the programing that takes place in our bodies. From the beating of the heart, voluntary muscles movement, to regulating body temperature and an ability to instantaneously perceive the world, the nervous system must be efficient, and extremely fast. From an animal perspective, the speed at which an external

stimulus (the sight of a predator, the smell of fire, etc) can be perceived and responded to, could be the difference between life and death. Thus, neurons have evolved to transmit signals at speeds between 5 and 120 m/s.[17,19,20]

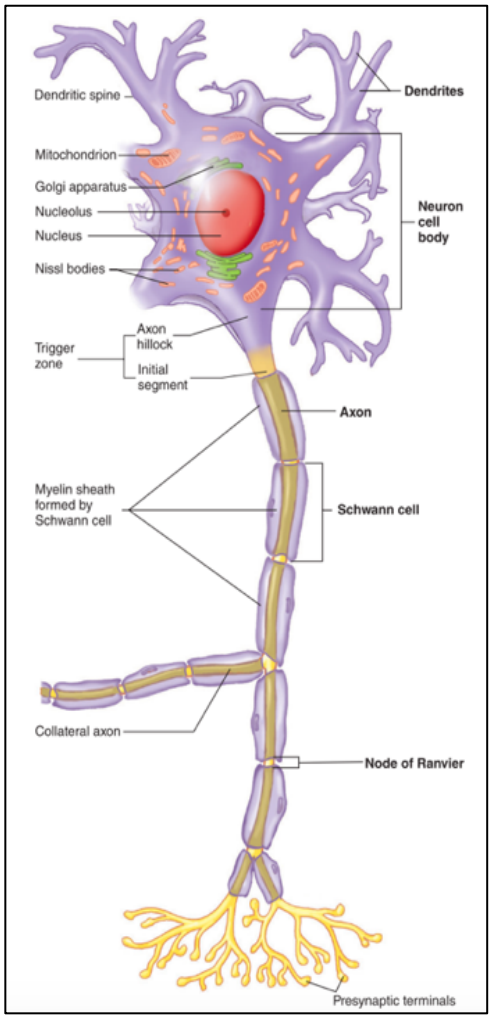

Figure 3 - Typical nerve cell. Action potentials arrive to dendrites and are propagated by the axon. Other organelles like nucleus, mitochondrion, and Golgi apparatus are commonly found in other cells. However the dendrites and axons are exclusive to nervous cells[17]

Action potentials are how neurons pass along the stimulus to the brain where it is perceived and appropriately responded to. The electrical properties of these cells must be emphasized to understand how action potentials are conducted. Certain cations (positively charged) and anions

(negatively charged) play vital roles in the normal functioning of cells. Under normal conditions, the inside of a cell (including neurons) is more negatively charged than the outer extracellular space. Specifically, the concentration of negatively charged molecules such as proteins, are much greater inside the cell than outside. In addition, the Sodium-Potassium pump, embedded within the cell membrane maintains an imbalance of charges by expending energy (1 ATP) to pump two positively charged potassium ions (K^+) against its concentration into the cell, while pumping three sodium (Na^+) against its concentration out of the cell.[17] The net imbalance of charges creates a resting membrane potential of around -70 mV in humans which can be measured as shown in Figure 4.

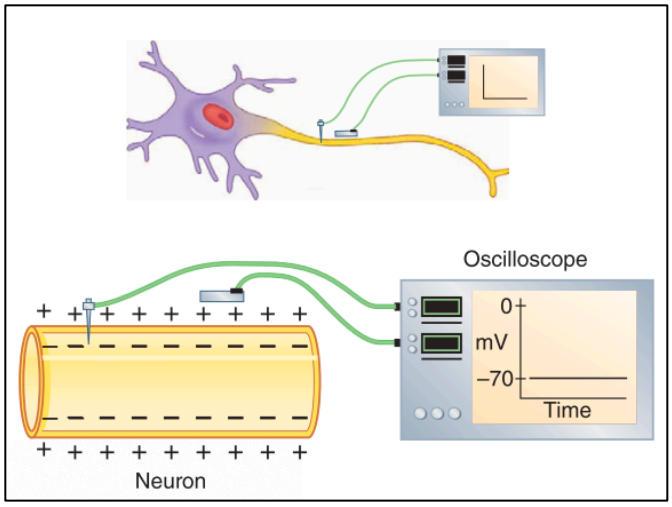

Figure 4 - The difference between the inside of the cell and the outside of the cell is referred to as the resting membrane potential and can be measured with an oscilloscope. [17]

In response to a strong enough stimulus or simultaneous arrival of multiple weaker stimuli, a neuron may undergo a phenomenon called an action potential. An action potential will result only if the stimulus is strong enough to trigger the neuron to a minimal threshold, and this threshold means that action potential conduction is an all-or-none principle. In response to a newly arriving stimuli, the cell membrane increases its permeability to sodium ions by opening ion channels. Once the previously restricted Na^+ ions are allowed to enter the cell, membrane potential will start to

increase. If the stimulus is strong enough (meets the threshold requirement) and enough Na^+ ions enter the cell then voltage-gated Na^+ channels (embedded within the cell membrane) open and more sodium flows into the cell (along its concentration) which causes the membrane potential to further increase, and subsequently more voltage gated Na^+ channels open in a positive feedback loop (a phase referred to as the depolarization phase). When the membrane potential reaches a maximum value, the voltage-gated Na^+ channels close, and the voltage gated K^+ channels open and allow for potassium to flow out of the cell (along its concentration) in a phase referred to as the repolarization phase. Finally, the previously mentioned Na^+/K^+ pump restores the resting membrane potential to bring an end to the action potential experience for that segment of the axon. The totality of the previously mentioned events is referred to as an action potential with the typical electric potential profile as shown in Figure 5.

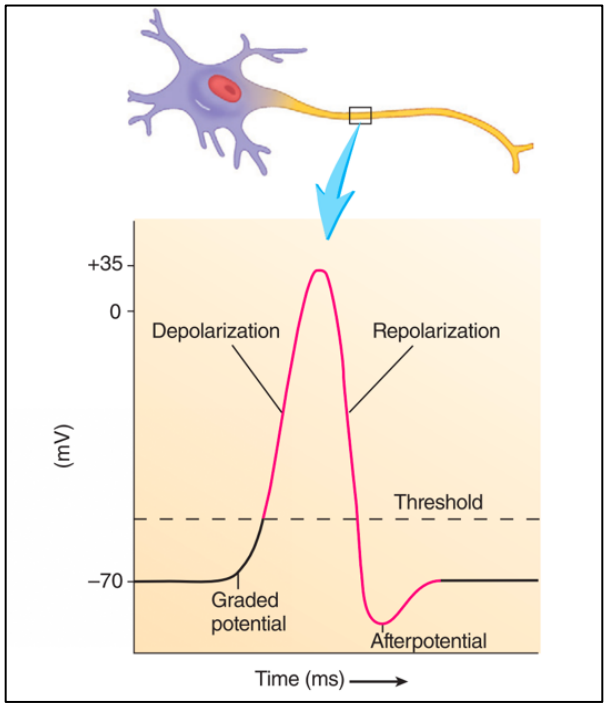

Figure 5 - The stages of action potentials. A graded potential is the sum of multiple stimuli which eventually are sufficient for the threshold at which point the action potential is triggered.[17]

1.2.3 Action Potential Propagation

In the previous section, attention was given to how action potentials are initiated in a neuronal cell in response to a sufficiently strong stimulus. However, it is also important to discuss the propagation of the action potentials and how one axon transfers an action potential to the next neuron. The action potential previously mentioned, occurs in a very small area of the membrane, and not throughout the whole membrane at once. Similar to a domino effect, the action potential is propagated forward as seen in Figure 6. The depolarization of an initial segment of the membrane would be enough to cause the threshold potential in an adjacent segment of the membrane. Thus, in this manner, the action potential is propagated forward. To ensure that the action potential is propagated only in one direction, there is an absolute refractory period (time needed for the Na^+/K^+ pump to restore the resting potential following the repolarization phase) which prevents the stimulation in the direction towards where the action potential originated. Furthermore, as seen in Figure 5, in the aftermath of the action potential, since the membrane potential is even more negatively charged than the resting potential it requires a higher level of excitation to trigger another action potential. This is another way which the action potential is directed only in the forward direction.

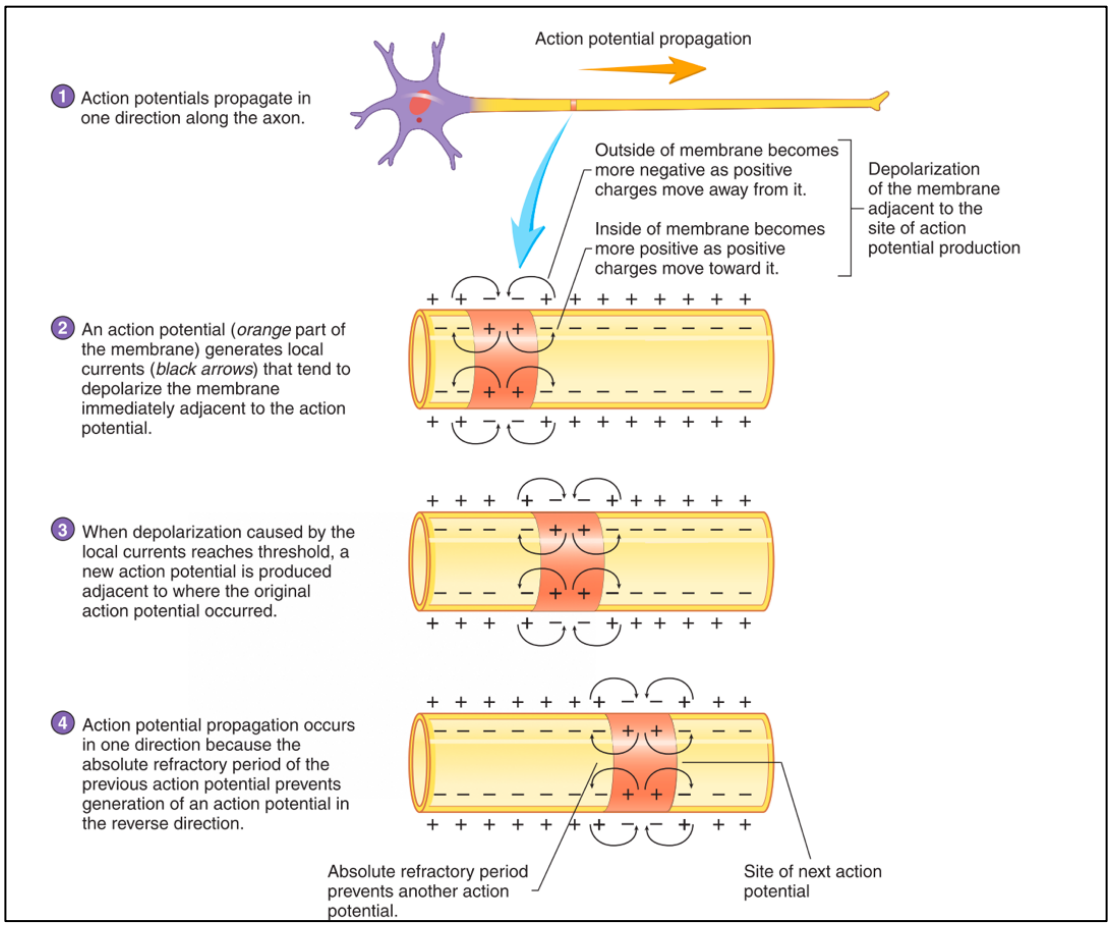

Figure 6 - Diagram demonstrating the domino-like process of action potential propagation.[17] *Action potentials generate local currents which depolarize the adjacent segment of the neuron. Once the threshold potential is reached for the new segment of the neuron, another action potential is generated. The refractory period ensures that the action potential propagates in one direction only.*

1.2.4 Synapsing – Neuronal Communication

Once the action potential has reached the end of the axon, it needs to be transmitted from one neuron to the next. This is done via a process referred to as a synapse.[17] Synapses fall into two categories, which are electrical and chemical.[17] Electrical synapses are not common in the nervous system of vertebrates but are found in human cardiac tissue. They work by connecting adjacent cells by structures called connexons, and essentially synchronizing the cells' activity.[17] Chemical synapses are more common, and function by releasing chemicals (neurotransmitters) from the axon

experiencing the action potential, through a synaptic cleft (extracellular space that is approximately 20 nm wide). The neurotransmitter then binds to its specific receptor which is found on the cell membrane of the adjacent neuron.[17] The binding of the neurotransmitter to the ligand-gated channels could trigger/inhibit an action potential, depending on the nature of the neurotransmitter.[17]

Neurotransmitters are vital to the functioning of many medications and illicit drugs. For example, the presence of the neurotransmitter dopamine is normal to the daily functioning of the human body and responsible for euphoric feeling.[17] However, cocaine competes with dopamine symporters by blocking them, and thus creates a scenario in which dopamine levels in the synaptic cleft are increased, resulting in an overstimulation in the postsynaptic neuron which can result in psychotic effects.

Similarly, another class of neurotransmitters called endorphins, bind to endorphin receptors on presynaptic neurons to block the release of a substance called substance P.[17] Substance P, a 10 amino acid polypeptide acts as a neurotransmitter to enhance the feeling of pain.[17] Opiates commonly prescribed for pain management, bind to the endorphin receptors and reduce pain by further blocking the release of substance P.[17] Therefore, for chronic pain management, both the propagation of the action potentials, and the functioning of the synapse can be modulated to improve patient symptoms.

1.2.5 Acute and Chronic Pain

As previously discussed, acute pain plays a role in promoting healing in response to injury. However, what happens when the injury has healed, but pain persists? For some medical conditions, persistent pain can be a sign of ongoing disease processes, however most often, chronic

pain is neither useful nor does it promote healing.[7] Although quite complex (refer to the article by Feizerfan & Sheh (2015) for an in depth review on the development of CP[21]), it seems repetitive nociceptive stimulations lead to pathophysiological changes in the pain pathways, including increased excitability and a lowered pain threshold.

1.3 Thermal Damage of Nerves

Applying sufficient heat to biological tissue/cells can have various effects which are of interest in medicine. Effects like increased cell membrane permeability, protein denaturing, and eventually cell killing due to heat are not uncommon, and in the case of cancer therapy are desired to help shrink tumours. Thermal therapy also applies to the management of chronic pain by locally applying heat to misfiring nerves. To quantify the amount of heat exposure, a concept called the thermal dose was developed and should be reviewed.

1.3.1 Thermal Dose

In 1984, Sapereto & Dewey developed a thermal dose model (Eq.1), which converts the time required to reach a certain biological endpoint at 43°C to the time that would be required to reach the same endpoint for any other temperature.[22] The unit for thermal dose is refered to as Cumalitive Equivalent Minutes at 43°C (CEM43°C). It is a simple relationship modeled by the following equation,

$$\mathrm{D} = \sum_{\mathrm{i}=1}^{\mathrm{n}} t_i \cdot R^{(43-T_i)} \quad , \qquad \text{(Eq. 1)}$$

where t_i is the *i*-th time interval, $R = 0.5$ when $T > 43$°C and $R = 0.25$ when $T < 43$°C, and T_i is the average temperature during the *i*-th time interval. Based on this if it takes 30 minutes at 43°C

to reach a certain biological endpoint, the same biological endpoint could have been reached in 15 minutes, if the temperature was 44°C instead.

1.3.2 Thermal Dose Threshold for Nerve Damage

Although data for the thermal dose required to block action potentials is limited, two particular studies helped to provide a framework to base a threshold on. In the first study authored by van Rhoon et al., (2013), a conservative threshold for thermal damage was decided on with a value of 9 CEM43°C was proposed.[23] This guideline was chosen because the thermal damage thresholds for human skin, muscle, fat and bone are all exceeding 9 CEM43°C.[23] In another study, Monafo & Eliasson (1987) used nerve conduction block as a biological endpoint and conducted thermal therapy (60 seconds to raise temperature from 37°C to 47°C and maintained at 47°C for 30 seconds) via RF currents on Sprague-Dawley rats' sciatic nerve.[24] Monafo & Eliasson (1987) found the treatment blocked nerve conduction in 67% of the animals.[24] While no CEM43°C was provided, it was calculated with Eq.1 (by taking a linear rise from 37 to 47°C over 60 seconds, and finding the CEM43°C value at each second, then finding the CEM43°C value of 47°C for 30 seconds and summing) to find the thermal dose threshold for nerves to be 10 CEM43°C. For this reason, it was decided that if PRF treatments block action potential propagation in nerves non-thermally, the thermal dose should be below 10 CEM43°C.

1.4 Applications of RF Currents in Chronic Pain Management

The first documented application of RF currents for thermal therapy dates back to the 1930s, and the first commercial RF generator was introduced in the 1950s.[25] Since then, it has gained popularity in treatment of tumours, and more recently, treating chronic pain.[25–28] The details will be outlined in the sections to come, but in short, RF therapy involves exposing a target region

(tumour or nerve) to an alternating current, in the radiofrequency (50-500 kHz) region.[27]. For chronic pain, RF currents have been used to target pain originating from various locations including, lumbar facet joint, cervical facet joint, sacroiliac joint, intervertebral disc, and dorsal root ganglion just to name a few.[25]

1.4.1 Continuous RF vs Pulsed RF

Traditionally, a clinician's aim when applying RF has been the local heating to block the nociceptive signals and thus block the perception of pain.[27] Clinicians locate the misfiring nerves radiographically and treat continuously for 60 – 90 seconds that result in electrode tip temperatures of 65 – 75°C to produce the desired lesion.[27] Treatment parameters are not standardized and there is some level of variation, associated with clinician experience and preference. For example, to treat the cervical facet nerve, a treatment of 80°C for 90 seconds was reported.[25] To treat the sacroiliac joint, a common source of lower back pain, RF treatment parameters that produced 60°C for 2.5 minutes were reported.[25] These treatments are carried out in continuous (CRF) mode with waveform seen in Figure 7.

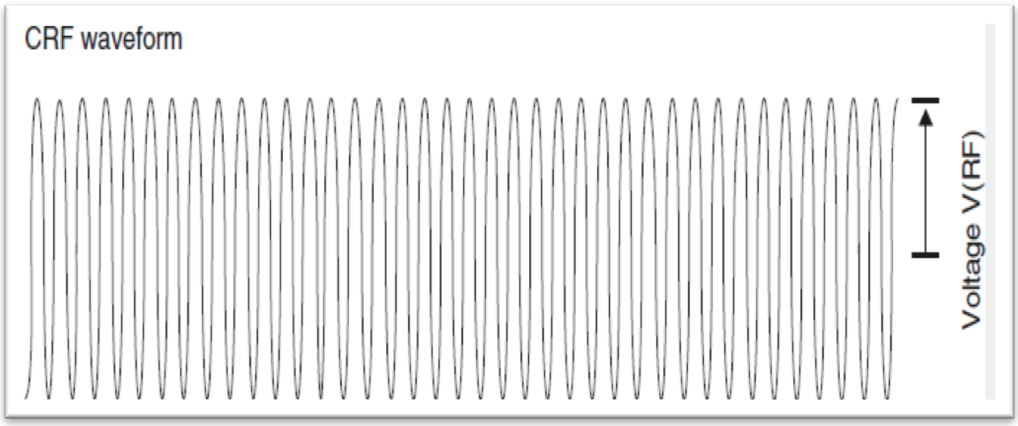

Figure 7 - Continuous RF waveform. In this mode, the aim is to create a thermal lesion.

Major downfalls of RF therapy include motor deficits due to damaging adjacent non-target nerves, and/or deafferentation syndrome.[26,27] Deafferentation syndrome pain is an undesirable outcome for patients who experience injury to the nervous system, with symptoms including spontaneous sensation of pain.[29] More recently, clinicians have been investigating the effects of pulsed RF (PRF) as an alternative to the continuous application of RF (CRF). As shown in Figure 8, rather than continuous flow of current the RF generator creates short current bursts (10-30 ms) between one and eight times per second.

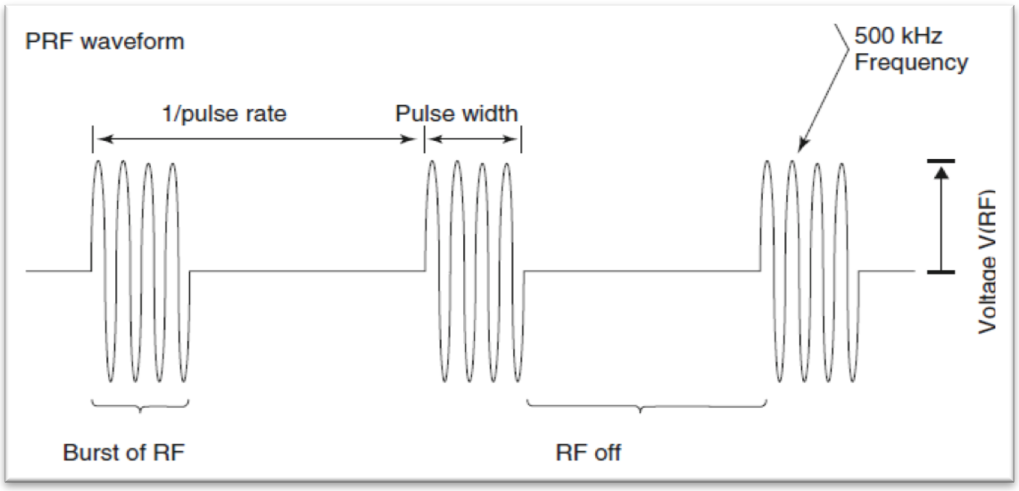

Figure 8 - Pulsed RF waveform. Typical pulse width is 10-30 ms, and typical pulse rate is 1-8 Hz.

A typical PRF treatment parameter is 20 ms pulse width at 2Hz.[26,27] Pulsing the current results in electrode temperatures less than 42-44°C,[25–27,30,31] falling below temperatures below CRF therapy. By allowing a relatively long time to pass between pulses, the heat can dissipate through conduction and convection (blood flow from nearby veins or arteries), with imperceptible discomfort, even in highly sensitive areas for which CRF treatment can be intolerable.[31] A

reduction in average temperature allowed clinicians to experiment with higher voltages when using PRF mode.[32]

PRF was developed after scientists began to wonder whether the effects of RF treatments are solely attributed to tissue heating, or whether the electric field or magnetic field play a role as well.[33] The exact mechanism of action of PRF is poorly understood,[27] however, electric field exposure is proposed to be responsible for the blocking effects.[32]

1.4.2 Monopolar vs Bipolar

The RF setup can fall under two categories. The first is called monopolar, in which one electrode is placed in the region of interest, and the circuit is completed with a grounding pad, outside of the body. The second setup is called bipolar where by two RF electrodes are placed around the targeted region. Both pictorial representation of the respective setups can be seen in Figure 9.

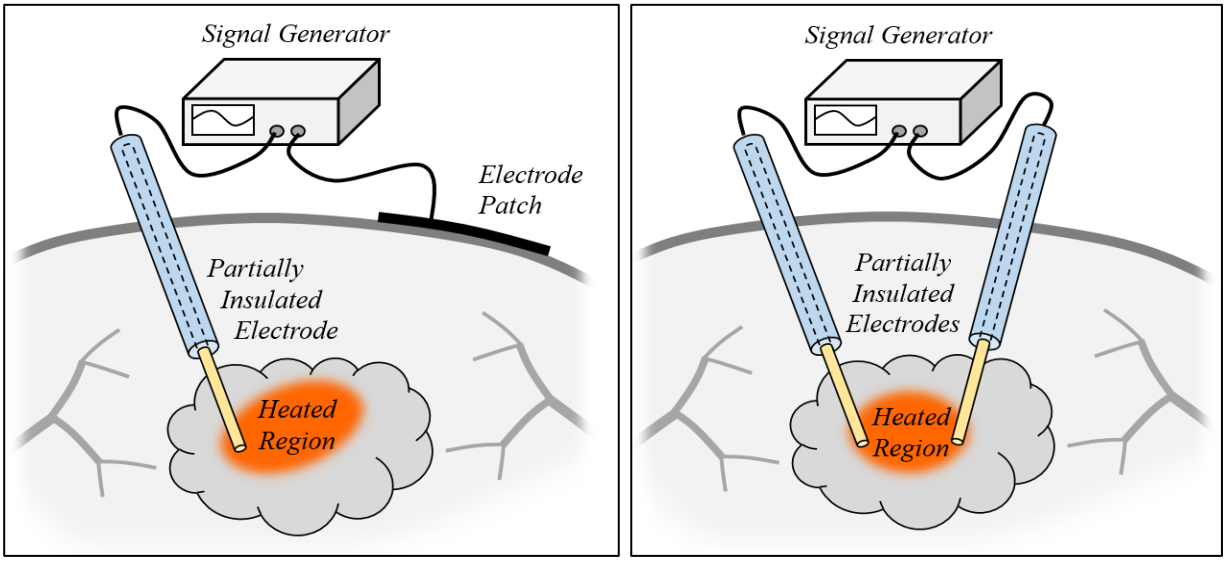

Figure 9 - Comparison of monopolar (left) and bipolar (right) RF treatments. Bipolar mode provides a larger heated region, however is doubly invasive.[39]

In the monopolar setup heat spreads axially and symmetrically, however the width of the affected area plateaus quickly within a few millimeters. This can make targeting the nerve

challenging in some anatomical locations and generally requires higher precision than bipolar RF. Although bipolar RF is twice as invasive (two probes are inserted instead of one), it leads to a larger heated area found between the probes. Bipolar mode is more suitable if the area around the target is large enough to accommodate both electrodes, allowing more room for error in electrode placement, and overall increased control over the treatment.

1.5 Hypothesis and Outline

This thesis proposes that pulsed radiofrequency (PRF) therapy can be used to block the propagation of action potentials, and when used for chronic pain management, deliver thermal doses below 10 CEM43°C. In order to confirm this hypothesis, the project was broken into four objectives: (i) conduct *in-vivo* animal experiments to analyze action potential propagation before and after PRF treatment to assess the efficacy of the treatment, (ii) create a computational model that simulated electrical field and heating of RF therapy, (iii) validate the model experimentally, and finally (iv) simulate clinical treatment parameters in order to analyze the thermal dose (Eq.1) delivered to the target.

2 Theory and Methods

In this chapter the electromagnetic phenomena relevant to RF therapy will be reviewed along with an introduction to the bioheat equation. Next, the methods for the action potential experiments and the methods for the computational simulations will be explained, including the approach to validating the simulation methodology. Finally, a description of how the simulations were used to simulate two realistic scenarios is provided.

2.1 Theoretical Background

RF therapy is governed by two main partial differential equations. One solves for electric field and the other to solve for the temperature change over time.

2.1.1 Electromagnetic Background

Starting with one of Maxwell's equations, specifically Amperes law:

$$\nabla \times \mathbf{H} = \mathbf{J} + \frac{\partial \mathbf{D}}{\partial t} \quad , \qquad \text{(Eq. 2)}$$

where **H** represents the magnetic field (A/m), **J** represents current density (A/m^2), **D** represents the electric displacement (C/m^2) and *t* represents time.[34] Next, the divergence of both sides of Equation 2 is taken,

$$\nabla \cdot (\nabla \times \mathbf{H}) = \nabla \cdot (\mathbf{J} + \frac{\partial \mathbf{D}}{\partial t}) \quad , \qquad \text{(Eq. 3)}$$

and since the divergence of the curl is always 0, we get

$$0 = \nabla \cdot (\mathbf{J} + \frac{\partial \mathbf{D}}{\partial t}) \, . \qquad \text{(Eq. 4)}$$

The time-derivative can be eliminated by using frequency domain representation via Fourier transform

$$0 = \nabla \cdot (\mathbf{J} + i\omega\varepsilon_0\mathbf{D}) . \qquad \text{(Eq. 5)}$$

Eq. 6 is derived from the relationship between electric displacement **D** (C/m^2) and electric field **E** (V/m) where $\mathbf{D} = \varepsilon\mathbf{E}$

$$0 = \nabla \cdot (\mathbf{J} + i\omega\varepsilon_0\varepsilon\mathbf{E}) , \qquad \text{(Eq. 6)}$$

where **E** represents the electric field (V/m), $i = \sqrt{-1}$, $\omega = 2\pi f$, ε is the relative permittivity of the tissue, $\varepsilon_0 = 8.85 \times 10^{-12}$ F/m is the permittivity of free space.[32]

Considering the relationships between electric field **E** (V/m) and potential Φ (V), and current density **J** (A/m^2) and electric field. The relationships are as follows:

$$\mathbf{E} = -\nabla\Phi \quad \text{and} \quad \mathbf{J} = \sigma\mathbf{E}$$

where σ represents the specific electrical conductivity of the tissue (S/m). Using these two relationships, Eq. 6 can re-written as follows:

$$0 = \nabla \cdot (\sigma\mathbf{E} + i\omega\varepsilon_0\varepsilon\mathbf{E})$$

$$0 = \nabla \cdot [(\sigma + i\omega\varepsilon_0\varepsilon)\mathbf{E})$$

$$0 = \nabla \cdot [(\sigma + i\omega\varepsilon_0\varepsilon)\nabla\Phi] \qquad \text{(Eq. 7)}$$

Eq. 7 can calculate the potential and electric field at points in space surrounding an RF electrode, using a computer program capable of finite element method analysis.

2.1.2 Bioheat Equation

The bioheat equation (Eq. 8) is a partial differential equation that can be used to model the heat transfer in tissues over time.[32] The equation is as follows:

$$\rho C_\rho \frac{\partial T}{\partial t} = P + \nabla \cdot (k \nabla T) + W_b C_b (T_b - T) \ , \qquad \text{(Eq. 8)}$$

where ρ represents mass density (kg/m^3), C_ρ represents the heat capacity of the material (J/kg °C), k represents the thermal conductivity of the medium (W/m °C), W_b represents mass flow density for blood (kg/m^3 s), $C_b$represents the specific heat of blood, and T_b represents the normal temperature of blood (37°C). More generally, the term on the left ($\rho C_\rho \frac{\partial T}{\partial t}$) represents the rate of change of heat energy density, the first term on the right (P) represents the power deposition density (W/m^3), the second term on the right ($\nabla \cdot (k \nabla T)$) represents the conductive heat loss per unit volume, and the final term on the right ($W_b C_b (T_b - T)$) represents the heat loss from blood convection.

The electromagnetic equation and the bioheat equation are coupled together through the average power deposition density term, which can be written as a function of current density and or the electric field amplitude:

$$P = \frac{|\mathbf{J}|^2}{2\sigma} = 0.5\sigma |\mathbf{E}|^2 \, , \qquad \text{(Eq. 9)}$$

which oscillates with the RF frequency.

Creating a simulation governed by the equations discussed above, would allow for analysis of heating patterns, as well as electrical field distributions for any given geometry. The Boundary conditions include current conservation on the insulating material boundaries such that

$\mathbf{n} \cdot (\mathbf{J_2} - \mathbf{J_1}) = 0$ and the conducting material at the active tip boundary should follow $\mathbf{n} \times (\mathbf{E_2} - \mathbf{E_1}) = 0$ since the electric field is continuous across boundaries. The boundary conditions dictate that electric field lines point parallel to the insulating material and normal to the conducting material.

2.2 In-vivo Experiments of Nerve Blocking by PRF

One aim in this project was to conduct *in-vivo* animal experiments to investigate how PRF effects action potential propagation in functioning nerves. Due to time restraints, it was decided that the animal of choice would be the common earthworm (*Lumbricus terrestris*). Earthworms have large nerve cords relative to the size of their body and could be used to study action potential propagation with in-tact animals, not requiring any dissection. As an invertebrate animal, experiments on earthworms do not require animal ethics approval, as confirmed by Ryerson University and St. Michael's Hospital Animal Care Committee (ACC). To study the effects of PRF on earthworm nerves, measurements were taken of the nerves' ability to respond to electrical stimulation before and after treatment. The detailed experimental set up is described later in this section.

As seen in Figure 10, earthworms have one main nerve chord (the ventral nerve chord) responsible for flight reflexes and twitches, which spans the length of their body and is comprised of three individual giant fibers: one median (MGF) and two lateral (LGF).[35,36] The MGF fiber has a diameter up to 0.07 mm and the LGF has a diameter up to 0.05 mm. The two LGF fibers have segmental cross sections, and therefore are regarded as one functional unit.[35,36] These two nerve fibers are reported to have distinct conduction speeds (MGF ≈ 23 m/s and LGF ≈ 8 m/s).[35,36]

The nerves of intact, anesthetized earthworms can be stimulated by electrical impulses and measured by reading electrodes with the following experimental setup.

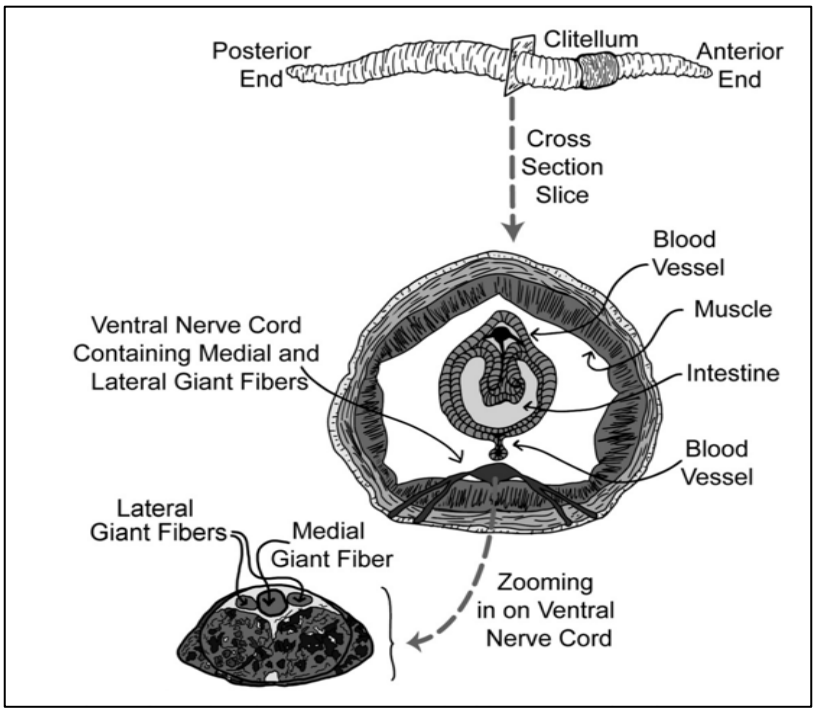

Figure 10 - General earthworm anatomy (top) with cross-section (bottom) zooming in on the ventral nerve cord with a view of the median giant fiber (MGF) and lateral giant fibers (LGF).[36]

2.2.1 Experimental Components

To trigger and record the nerve responses within the earthworm nerves, BIOPAC (Montreal, Qc) MP36 hardware and software were used. To treat the earthworms with PRF, we used URF-2AP RF generator courtesy of Diros Technology Inc (Markham, On) was used (Figure 11).

2.2.1.1 BIOPAC Electrophysiology System

Stimulating and reading electrodes (part number EL450 stainless steel needle) are connected to the MP36 hardware with ELSTM2 and BSLCBL8 adaptors respectively. The hardware is connected to a computer by USB and accompanied by a user-friendly software. This data acquisition unit is capable of triggering impulses (0 – 10 V and pulse width as little as 0.05 ms) and recording the response potential with a sampling rate up to 10^5 Hz with a sensitivity as low as 0.1 μV. The system

was used to generate compound action potentials in the two nerves of the earthworm and to record the respective response.

2.2.1.2 RF Generator

The RF generator used to treat the earthworm nerves was model URF – 2AP and the RF probes were the thinnest available (21 Gauge). This machine is capable of delivering continuous and pulsed RF (pulse width of 10, 20, or 30 ms and a pulse repetition rate between 1 Hz – 8 Hz) for up to 120 seconds at a time. It is worth noting that this machine does not allow the user to specify the voltage, rather it has a power control which must be adjusted manually, and the current is ramped up to a maximum value. The RF electrodes also contain thermocouples to monitor temperature and allow the user to set a maximum tip temperature that modulates the RF output, however for the purposes of this study, this functionality was ignored after it was decided that the precision (of 1°C) was insufficient.

Figure 11 - Diros Technology Inc OWL URF-2AP RF generator.

2.2.1.3 Animal Preparation

Fresh earthworms were acquired from a local fishing shop in Toronto, Ontario. They were stored in a refrigerator when not in use, and always released to the wild if not used by 6 weeks. Earthworms were placed in an anesthetic solution (10% ethanol prepared by diluting 40% ethanol vodka) for ~5 minutes or until no response was seen when tapping the head and tail of the animal with a plastic probe, as per methods previously outlined.[36] Once the animal was anesthetized (lasting 5-15 minutes), it was removed and washed under tap water for several seconds to remove a secretion-like substance from the earthworm before being placed on a platform that was created for this project. Occasionally, the anesthesia would wear off and the animal would begin to show signs of movement, at which time a cotton swab sprayed with the anesthetic solution was brushed on the animal to anesthetize it once more. In other cases, the anesthesia was lethal for the animal, and this was observed by no initial response to even the strongest stimulus (10 V). Furthermore, throughout the experiments, earthworms were brushed with moist swabs to ensure good electrode contact and prevent the complete drying out of the animal.

2.2.2 Experimental Setup

As seen in Figure 12, a Styrofoam platform was created which would ensure that all electrodes were positioned in a stable manner. This was achieved by pushing the electrodes through the porous Styrofoam until only the tip was seen on the other side.

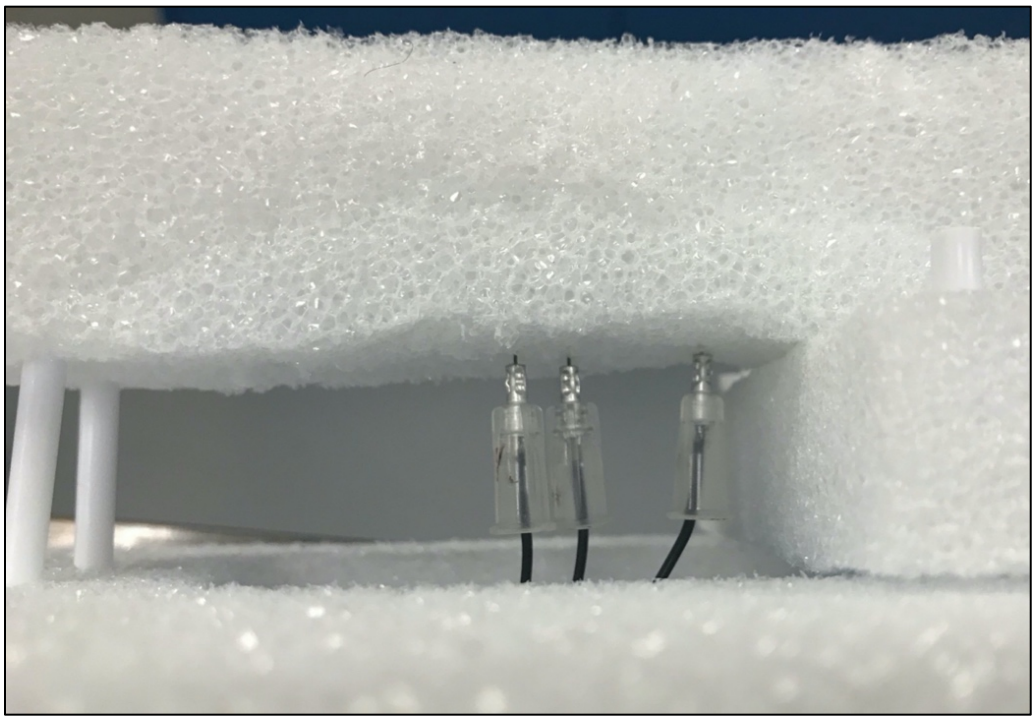

Figure 12 - A porous Styrofoam platform was cut to a size that could allow the tip of the electrode to penetrate fully and pierce through. Once the electrodes were pushed through, they were fully stable with no adhesive required.

The components were connected as shown in Figure 13 and the anesthetized worms were placed on the platform with the electrodes penetrating the body of the earthworm. The stimulating electrodes were always placed posterior to the well recognizable clitellum (see Figure 10). A grounding pad (tin foil attached to alligator clips) was used. To reduce noise, the platform was isolated as much as possible by maximizing the distance to the nearby computer and electronics.

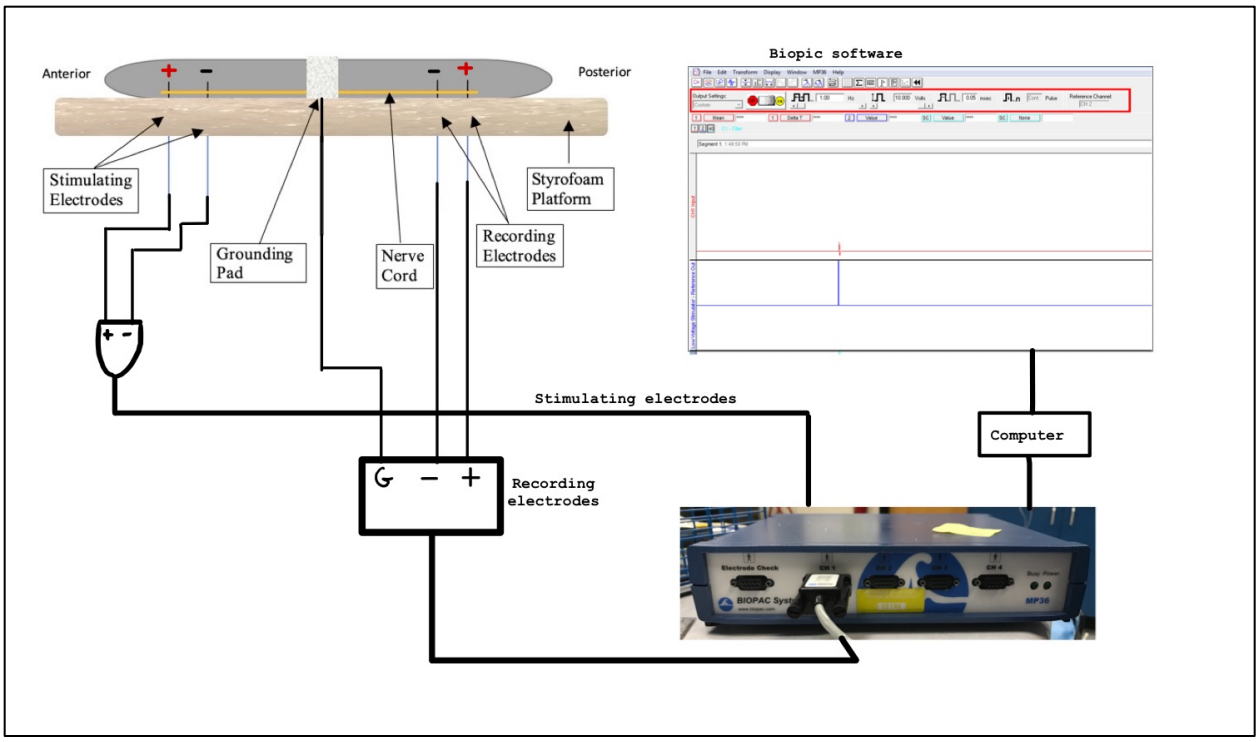

Figure 13 - Schematic set up of the earthworm action potential acquisition.

Once the worm was in position, 0.05 ms electrical pulses were sent through the stimulating electrodes using the BIOPAC software to trigger nerve response. For each worm, the pulse magnitude was increased in 0.1 V increments until the stimuli had reached the threshold level to illicit a response from both nerves (4 V – 7 V) as shown in Figure 14.

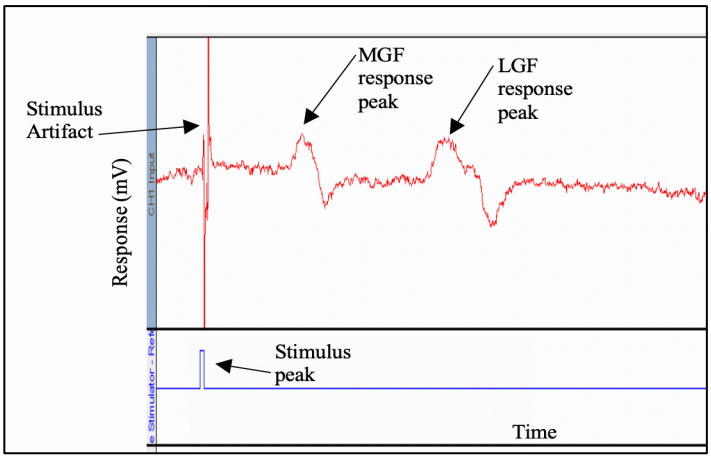

Figure 14 - A screenshot from the BIOPAC software. In blue is the stimulus peak of 0.05 ms. It corresponds to the stimulus artifact that is recorded in red by the reading electrodes. The response peaks for both nerves are also labeled.

The time the compound action potential to propagate along the nerve from the stimulating artifact and the nerve response peaks depends on the distance from the second stimulating electrode and first recording electrode. Using a caliper, the distance between the two electrodes was measured as 5.23 cm apart. Knowing the distance and the time it takes for the peak to appear, the conduction velocity of the nerves can be checked for validation with values found in literature.

2.2.3 Treatment Conditions

After the initial response was recorded, the grounding pad was removed, and the RF probes were raised from within the Styrofoam as seen in Figure 15 and inserted into the earthworm. To investigate the effectiveness of PRF on action potential, the magnitude of the peaks (peak value – baseline value) of each nerve were measured before and after PRF treatment. The baseline value was assumed to be the average value for the segment of noise that came before the nerve response. For the MGF nerve this segment was from the stimulus artifact until the MGF response, and for the LGF nerve this segment was from the end of the MGF response to the start of the LGF response. For each worm, 5 measurements were made every 30 seconds, prior to treatment, and 5 were made following treatment.

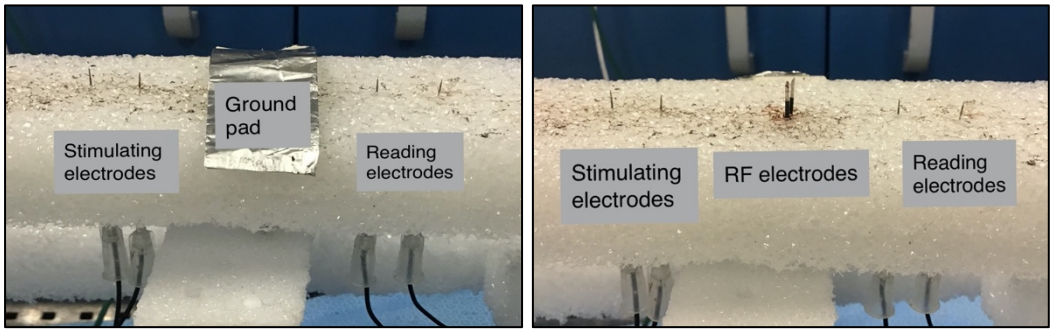

Figure 15 - The picture on the left shows the set up for BIOPAC measurements before and after treatment, and the picture on the right shows the setup during RF treatment

In order to ensure that the nerve is treated without risk of accidentally severing the nerve chord, bipolar mode was selected as the treatment setup. The RF probes located laterally on either side of the nerve chord as shown in Figure 16. 30 worms were divided into 3 treatment groups (V_{max} = 0 V, 35 V, and 70 V) and treated for 120 seconds with 20 ms pulse width and 2 Hz pulse frequency with the URF – 2AP RF generator.

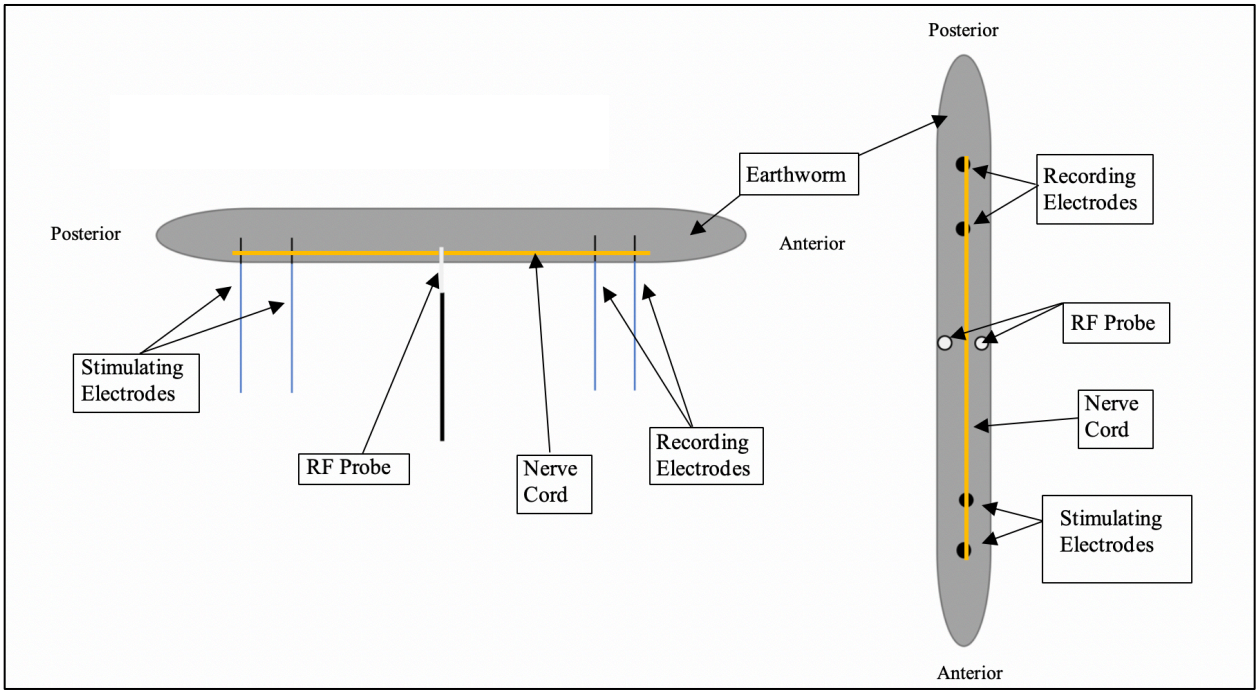

Figure 16 - Placement of the earthworm with respect to the various electrodes. All electrodes are stabilized by piercing through a Styrofoam platform. It is important that the RF probes can be inserted after acquisition by slightly elevating them through the platform of the initial response and that the stimulating and recording electrodes remain in the same position throughout the process.

It should also be noted that the RF probes were rather invasive for the earthworms and that for some worms, the active tip length was larger than the diameter of their body, resulting in a portion of the active tip being outside of the worm's body. However, it was ensured that the treatment was not lethal for the worms, by allowing the anesthesia to wear off and then observing the earthworm for movement in the head area.

2.3 Simulations

Since partial differential equations model RF therapy a finite element simulation was created using COMSOL Multiphysics, guided by the work of Cosman and Cosman (2005), to understand and investigate the thermal effects of PRF, however their simulation was two-dimensional and did not encompass the bipolar mode of treatment.[32] We modified their simulation from two-dimensional to three-dimensional, and also added the bipolar mode.

2.3.1 Monopolar RF Model

A 2D-axisymettric geometry was created which included a stainless-steel probe (radius of 0.35 mm) with a 5 mm active tip, and the rest surrounded by insulation (thickness of 0.05 mm). The probe was located in a beef liver.

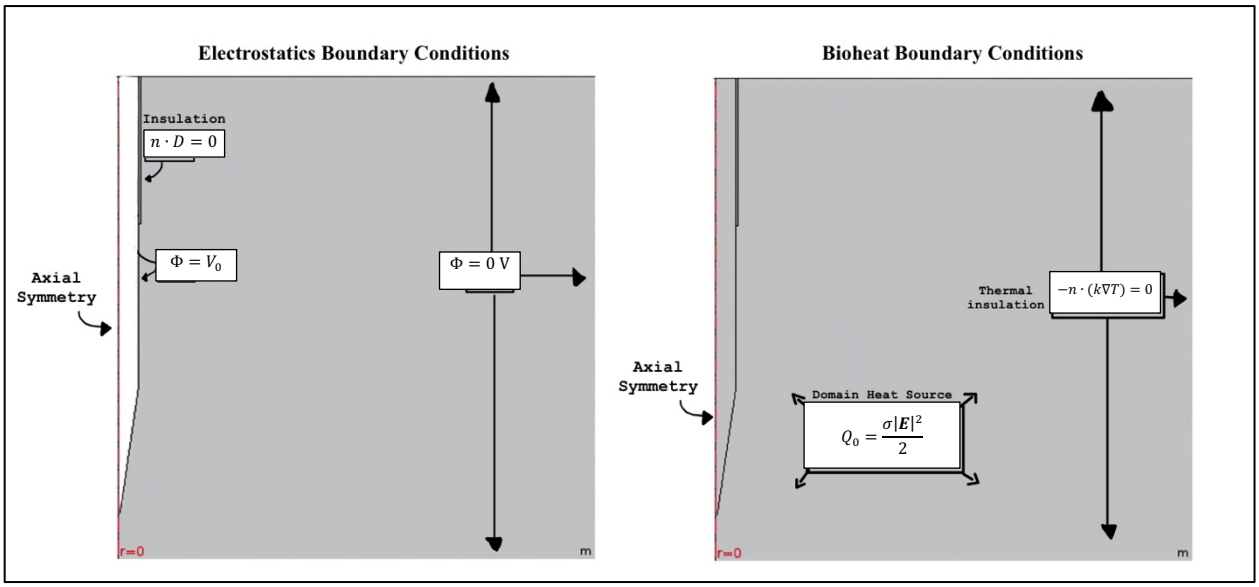

Figure 17 – 2D axisymmetric geometry with electrostatics (left) and bioheat module boundary conditions (right).

All material properties were the same as those used by Cosman and Cosman (2005) and can be found in Table 1.[32]

Table 1 - Material properties that were used for finite element calculations [34]

Material	Quantity	Value	(units)
Liver	C_p, heat capacity	3,400	J/kg °C
	ρ, density	1,000	kg/m^3
	σ, electrical conductivity	0.29*	S/m
	ε, relative permittivity	2,000	—
	k, thermal conductivity	1.2	W/m °C
	W_b, blood perfusion	10	kg/m^3 s
Insulation	C_p, heat capacity	3,400	J/kg °C
	ρ, density	800	kg/m^3
	σ, electrical conductivity	0	S/m
	ε, relative permittivity	2.7	—
	k, thermal conductivity	0.01	W/m °C
Stainless steel	C_p, heat capacity	500	J/kg °C
	ρ, density	7,900	kg/m^3
	k, thermal conductivity	15	W/m °C

2.3.2 Electromagnetics Modeling

Haus & Melcher (1989)[37] outline the conditions for an electroquasistatic approximation to be valid which resulting in

$$\frac{\mu_0 \varepsilon_0 L^2}{\tau^2} \ll 1 \qquad \text{Eq. 10}$$

Considering that $c = \frac{1}{\sqrt{\mu_0 \varepsilon_0}}$, with some rearranging, Eq. 10 can be rearranged such that

$$f \ll \left(\frac{c}{2\pi L}\right) .$$

For a typical RF active tip length of $L = 10$ mm, and a characteristic time $\tau = \frac{1}{2\pi f}$, the electroquasistatic approximation is valid if $f \ll 4.7 \times 10^9\ Hz$. Since RF generators frequencies

are typically 50-500 kHz, the electroquasistatic approximation was valid. The electrostatics module was used to calculate the electric potential (and electric field) distribution when the potential Φ is fixed to the RF voltage at the tip of the electrode, and the outer boundaries are defined as the ground where $\Phi = 0$ V.

2.3.3 Bioheat Modeling

To model the heating with respect to time, the bioheat *(ht)* module was used. The outer boundaries of the liver were assigned as thermal insulation ($-n \cdot q = 0$) and initial temperature of liver was set to 37°C. The power deposition term of the bioheat equation (Eq. 8) was coupled to the electric field strength using Eq. 9. To implement both the ramping up of the current from the generator, and the PRF functionality, the power deposition density term was modified. The specifics of how these modifications were made can be found in Appendix A.

2.3.4 Bipolar Simulation

Building on the framework from the 2D-axisymmetric model, a 3D model was created to implement the bipolar RF setup. The bipolar simulation was validated experimentally. Beef liver was acquired from a local grocery store and allowed to naturally reach room temperature before being used. The probe separation was measured with a caliper and a thermocouple was introduced in-between the probes. Treatments were carried out on the beef liver and the increase in temperature was recorded as a function of time. With the setup shown in Figure 18, time readings from the timer on the RF generator and temperature readings from the thermocouple were used to created temperature versus time plots. Experiments were conducted with three CRF treatments conditions (7 V, 13 V, and 16 V) and two PRF treatment conditions (70 V, 90 V with 2Hz pulse rate, and 20 ms pulse width). Each condition was carried out three times for accuracy.

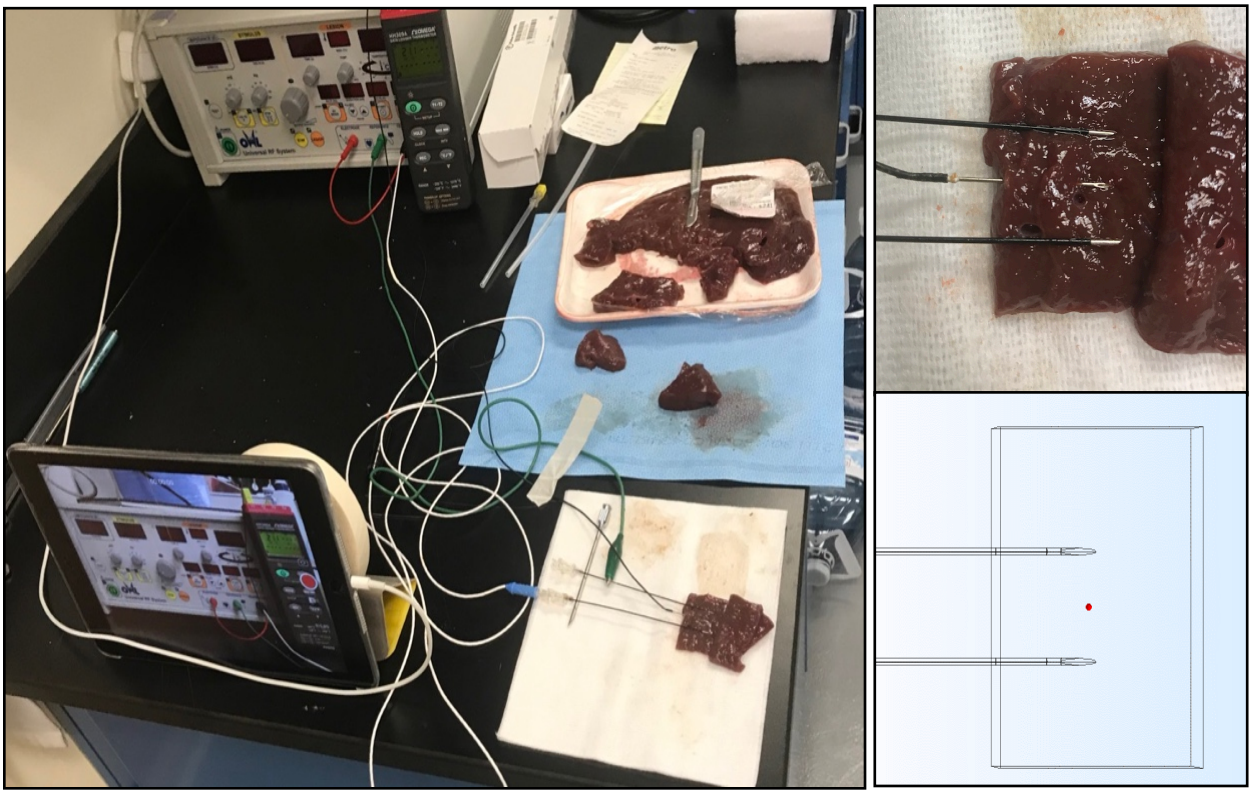

Figure 18 - On the left is the experimental setup for validation experiments. An iPad was used to record the RF generator and thermocouple reader during treatment. Afterwards the video was used to create a temperature-time profile. The image on the top right shows the thermocouple placed in the middle of the RF probes. On the bottom right is the COMSOL simulation of our experiment. The red dot indicates the location of interest which was used to acquire temperature-time profile.

The treatment parameters (peak voltage, ramp time, probe separation, and initial temperature) were used in the model to simulate the treatment. Temperature versus time profile at the location of the thermocouple was produced. After the simulation, the location of the thermocouple was selected as a point of interest, and the temperature vs time profile of that specific point was exported to Microsoft Excel. Although the simulation output included temperatures for each second of treatment, only those data points that corresponded to the experimental temperature rise were graphed to compare experimental and simulated results.

Table 2 - Sample of results for first 16 seconds of a liver treatment. Only the times at which a change in temperature was measured (highlighted data) were matched up with simulated times and both were plotted to compare. Times at which no change in temperature were detected were not plotted.

Time	Measured Temperature °C	Simulated Temperature °C
0	20.6	20.6
1	20.6	20.60136997
2	20.6	20.60540167
3	20.6	20.6126627
4	20.6	20.62338179
5	20.6	20.63940654
6	20.6	20.66008587
7	20.7	20.68541977
8	20.7	20.71439875
9	20.7	20.74488608
10	20.8	20.7785113
11	20.8	20.81527441
12	20.8	20.85517541
13	20.8	20.8982143
14	20.9	20.94439108
15	20.9	20.99370575
16	20.9	21.04668247

2.3.5 Earthworm Simulation

Finally, we simulated the earthworm experiments by creating a cylinder (5 mm radius and 12 cm length). The bipolar RF needles were placed 35 mm apart within the cylinder, as shown in Figure 19. The 70 V PRF treatment parameters from the earthworm experiment were simulated and the thermal dose at the location of the earthworm ventral nerve cord was calculated.

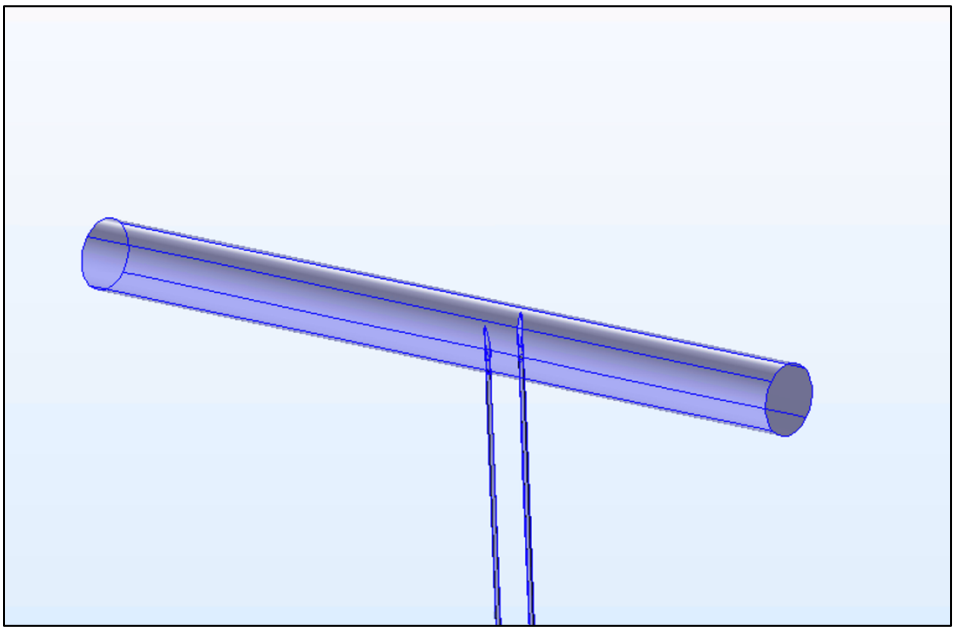

Figure 19 - The earthworm set up. Similar to experiments, the probes are inserted from the ventral side of the earthworm.

The heat capacity, density, relative permittivity, thermal conductivity, electrical conductivity, and relative permeability of earthworm tissue was assumed to be the same as beef liver.

2.3.6 Vertebra Simulation

The spinal region is a very common target for clinicians in the application of RF. As seen in Figure 20, the C6 vertebra geometry was modeled (C6 vertebra STL mesh; application ID 30951 from COMSOL library) in order to assess the thermal effects of PRF in realistic scenarios.

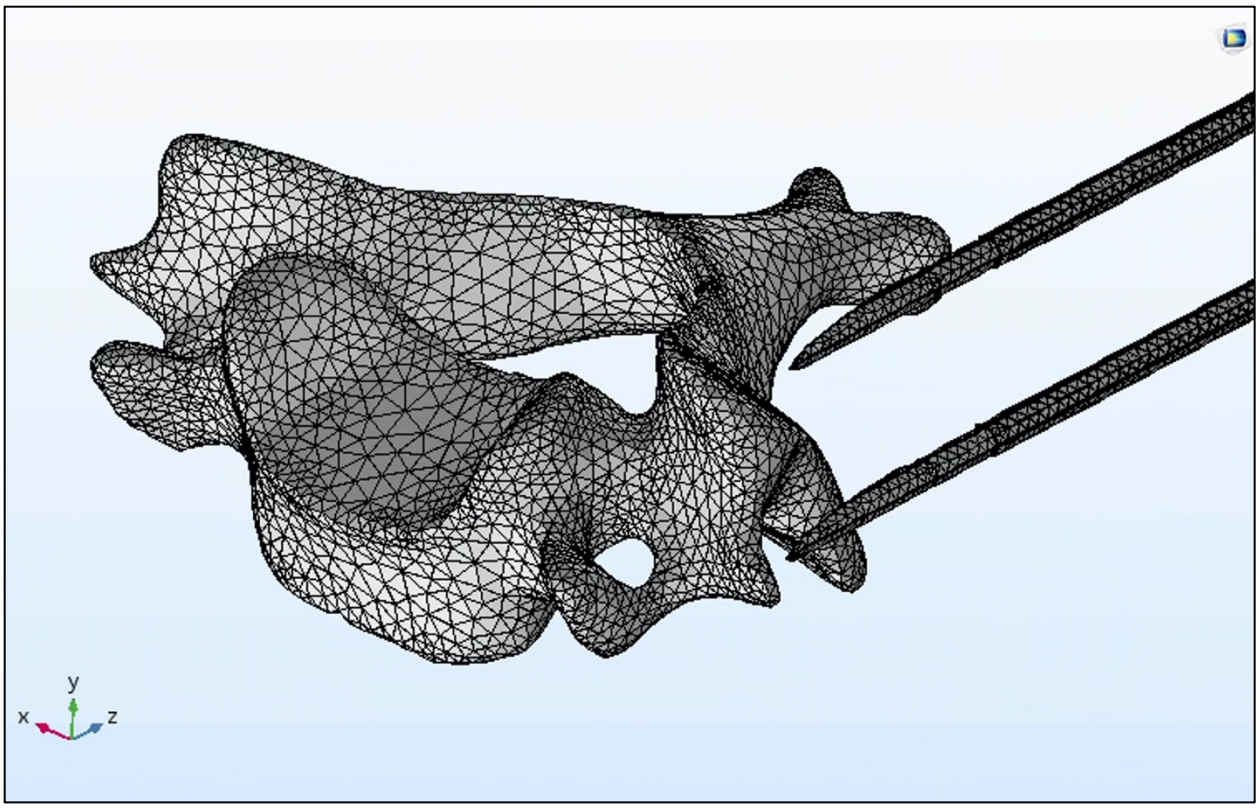

Figure 20 - C6 vertebra mesh and geometry as found on COMSOL with our RF electrodes implemented.

The mesh file was imported and converted into a solid with the material properties of bone. Around it was a cubical domain which was assigned material properties of muscle from COMSOL's material library. Bipolar RF probes were placed between the superior articular process and the transverse process to reach the target, which is where the medial branch of the dorsal ramus nerve root would be.[38] Clinical PRF treatment conditions were modeled including 20 ms pulse width (2Hz), for a duration of 120 seconds, at 45V.[38] Although the nerve itself was not explicitly included, its expected location was used to track the temperature rise in order to determine the thermal dose to the nerve (Figure 21).

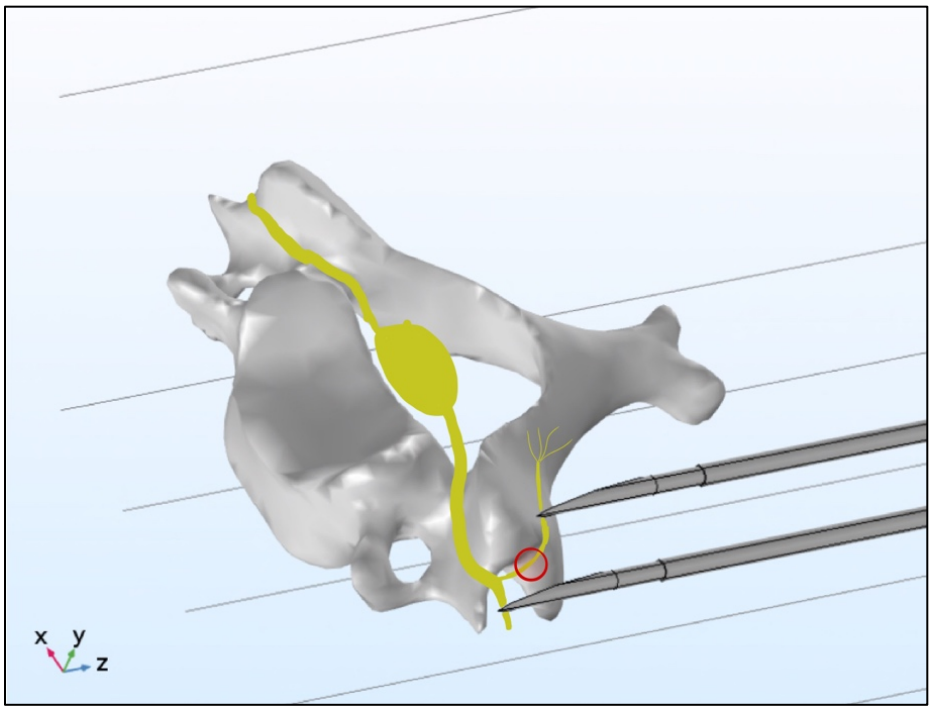

Figure 21 - The bipolar RF probes located such that they would treat the medial branch of the nerve. The nerve (yellow) and the target (red) are added to better illustrate the scenario. They were not however actually simulated in our model

3 Results and Discussion

The results are broken into two main segments. The first is from PRF earthworm experiments used to assess the efficacy of PRF treatment on action potential, and the rest are simulation related results to assess thermal doses.

3.1 *In-vivo* Experiments of Nerve Blocking by PRF

To investigate the effects of PRF on the earthworm nerves, we first had to be confident that the BIOPAC responses were in fact the responses from the nerves. This was done by comparing the experimental measurements for conduction velocity with those found in literature. Next, we evaluated the efficacy of PRF treatment by comparing the peak value of each nerve before treatment and after treatment.

3.1.1 MGF and LGF Conduction Velocity

Since the distance between the electrodes was measured to be 5.23 cm, the time from the stimulus artifact to nerve response peak were used to calculate the conduction speed of the nerves. Using 30 earthworms the conduction speed was measured to be 21.06 ± 3.2 m/s for MGF and 8.51 ± 1.8 m/s for LGF. These results are within 7.6% and 12% of previously reported MGF and LGF conduction speeds reported in literature (22.8 m/s and 7.6 m/s respectively).[36] These results led me to assume that the conduction in the two nerve fibers could be simultaneously measured.

3.1.2 PRF Treatment on AP Propagation

The magnitude of each nerve fiber response was recorded with the BIOPAC software prior to and following the RF treatment and can be seen in Figures 22 – 24.

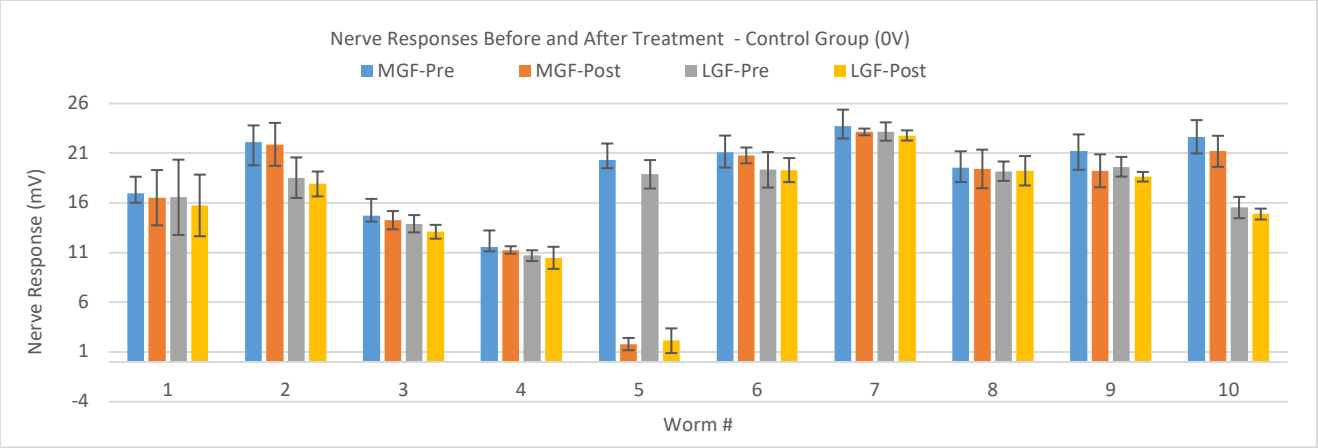

Figure 22 - Nerve response measurements for MGF and LGF nerves in earthworms before and after PRF treatment. This was the control group. RF probes were inserted as usual, but the voltage was set to 0V.

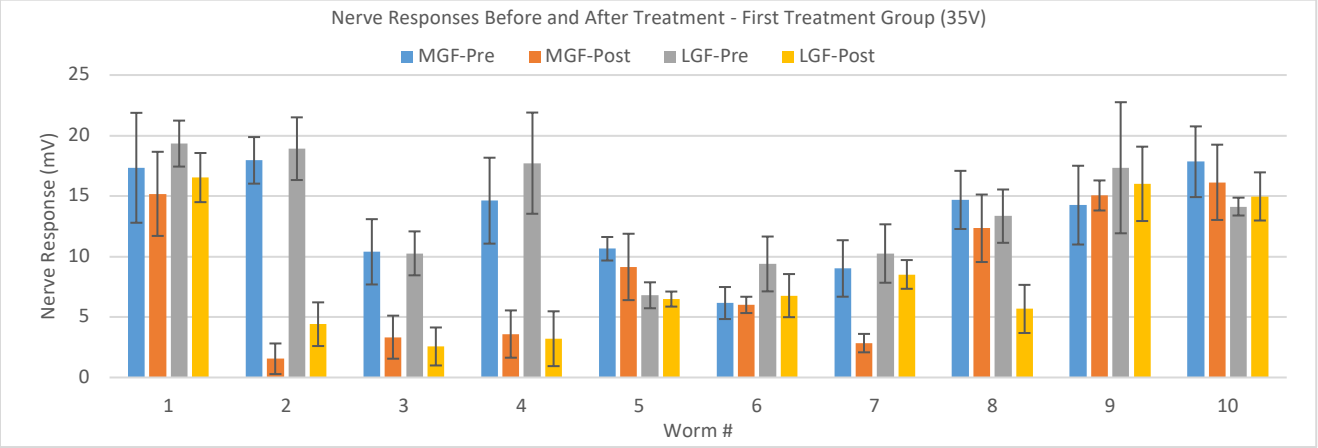

Figure 23 - Nerve response measurements for MGF and LGF nerves in earthworms before and after PRF treatment. This was the first treatment group of 35V.

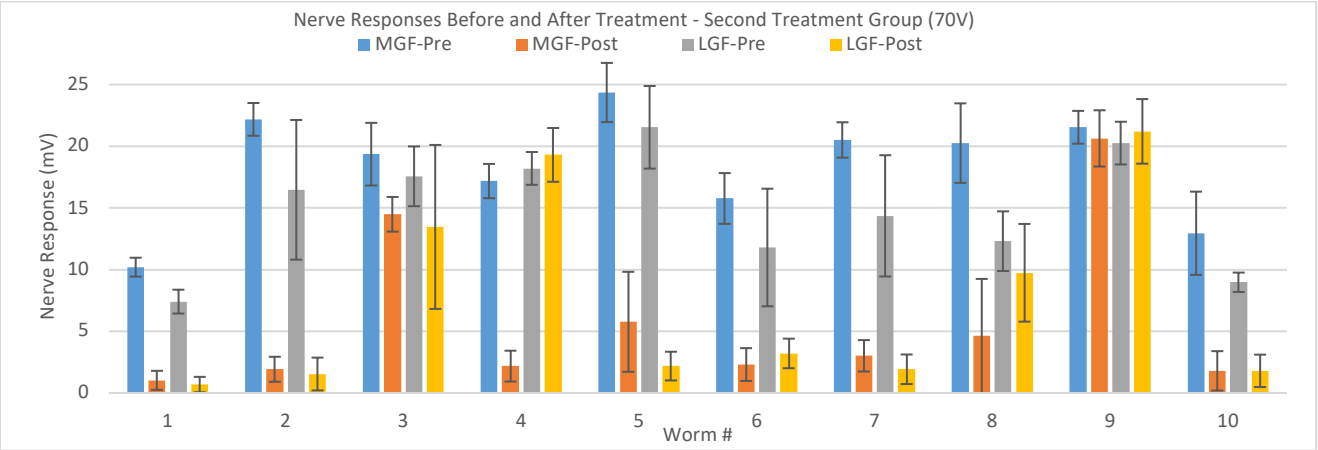

Figure 24 - Nerve response measurements for MGF and LGF nerves in earthworms before and after PRF treatment. This was the second treatment group of 70V.

In the control group, there was one worm (worm #5) that experienced a significant reduction in response peak voltage (92% reduction for MGF and 88% reduction for LGF). Excluding that worm, the remaining nine worms experienced an average of 3.3% reduction for MGF and 3.0% reduction for LGF. It is suspected that the outlier in the control group (worm #5) experienced this high level of reduction due unintentional dissection of the nerve when the RF probe was inserted into the earthworm, therefore it was excluded when determining PRF efficacy.

In the second treatment group (70V) 8 out of 10 MGF nerves and 6 out of 10 LGF nerves experienced a reduction of at least 50% which we assigned as the nerve block threshold. Interestingly, in some cases, it appears that only one of the two nerves were affected by PRF. To illustrate this point, we measured an 87% reduction with the MGF nerve but a 5% increase for the LGF nerve response for worm #4 of the 70V treatment group.

Figure 25 illustrates the efficacy of PRF treatments within the three groups, using 50% reduction as a criterion a blocked nerve.

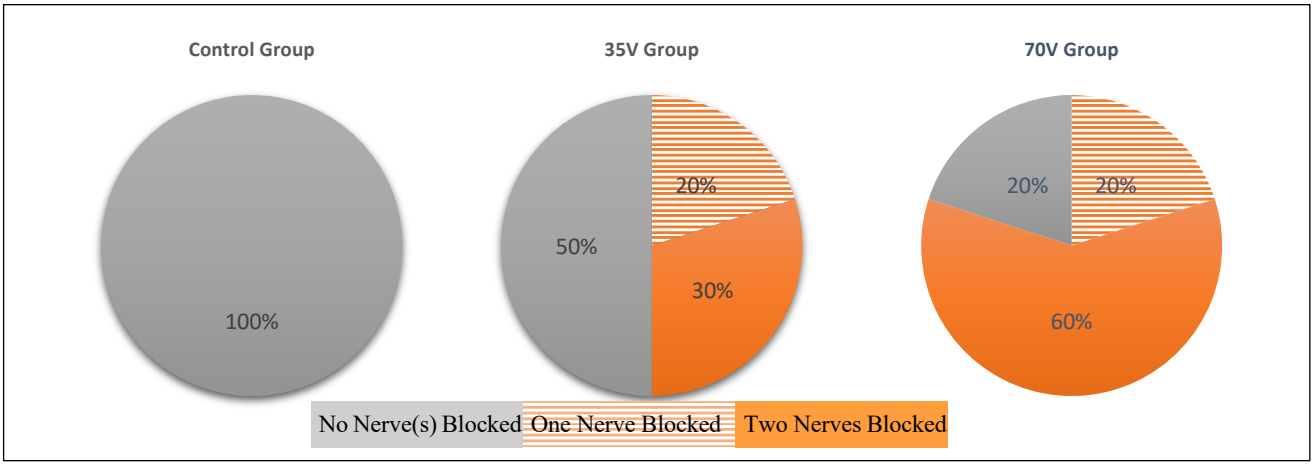

Figure 25 - Efficacy of PRF treatment on earthworm nerves. The criteria for nerve block was 50% reduction after PRF treatment.

Next, the percent reduction of all treated nerves were plotted on one graph as seen in Figure 26. With the exclusion of the outlier, all other control group animals experienced minimal

reduction (9.3 % maximum). In the 35 V group, some nerves were treated successfully and others that experienced minimal reduction which is why the orange data points are spaced with varying results. In the 70 V group, while some nerves experienced minimal reduction, there is a concentration of data points in >70 % reduction level.

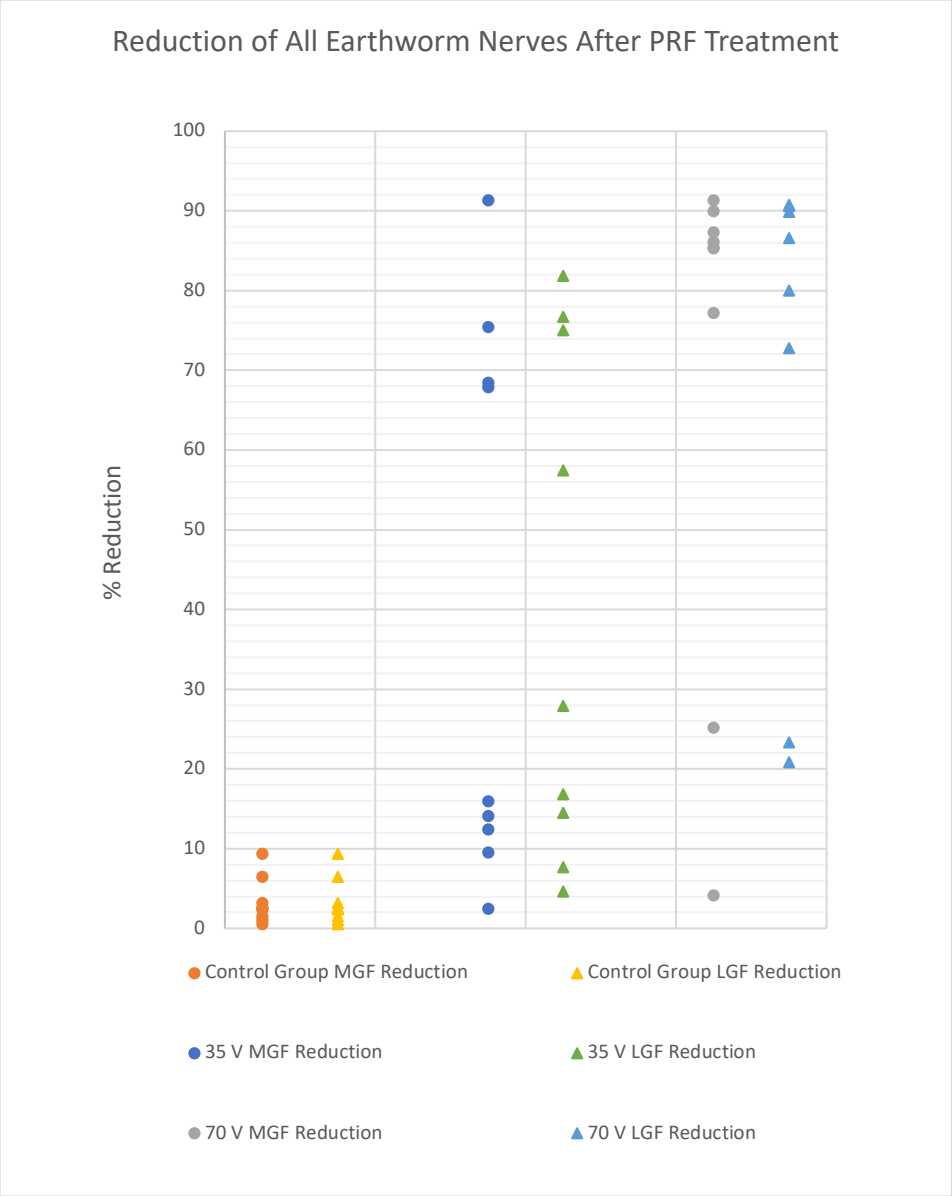

Figure 26 – All earthworm nerve data points represented on one graph. The data is concentrated on the low end (<10%) for the control group. When observing the 70V group, there is a high concentration of data points in the high end (>70%).

3.2 Simulations Results

In this section, we first visually compare and contrast our electric field and heating results with those of Cosman & Cosman (2005).[32] Next, we showed the results of our bipolar model validation. Finally, we evaluated the results of the earthworm simulation as well as the vertebra simulation for inspection of thermal dose at the target region.

3.2.1 Monopolar RF Model

The electric field of our simulation compared to the results of Cosman & Cosman (2005)[32] and is shown in Figure 27. The hotspots of the electric field can be found at the tip of the probe as well as the corner of the insulation where there is a sharp edge to the conductor. As expected, the electric field vectors orient outward, are parallel to the insulator boundary near the insulation and normal to the active tip. It should be noted that the gradient for the color scales are not perfectly matched, which explains the minor differences seen in Figure 27.

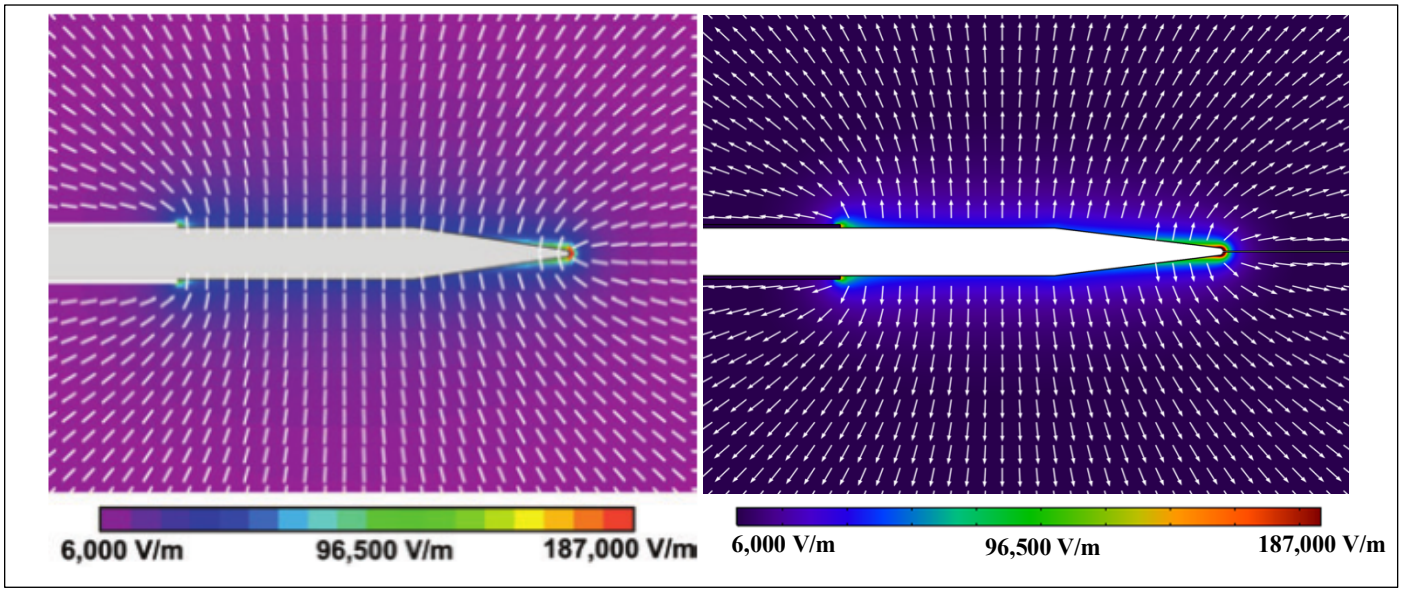

Figure 27 - Cosman and Cosman (2005) result for electric field with RF voltage of 45V (left) compared to the result from our model (right).

At the pointed tip, the curvature of the metal boundary is much higher, resulting in larger potential gradients $\nabla\Phi$ and thus intense electric fields (187,000 V/m). Figure 28 demonstrates how the intensity of the electric field falls off with $1/r$ dependence (r = radial distance from the axis).

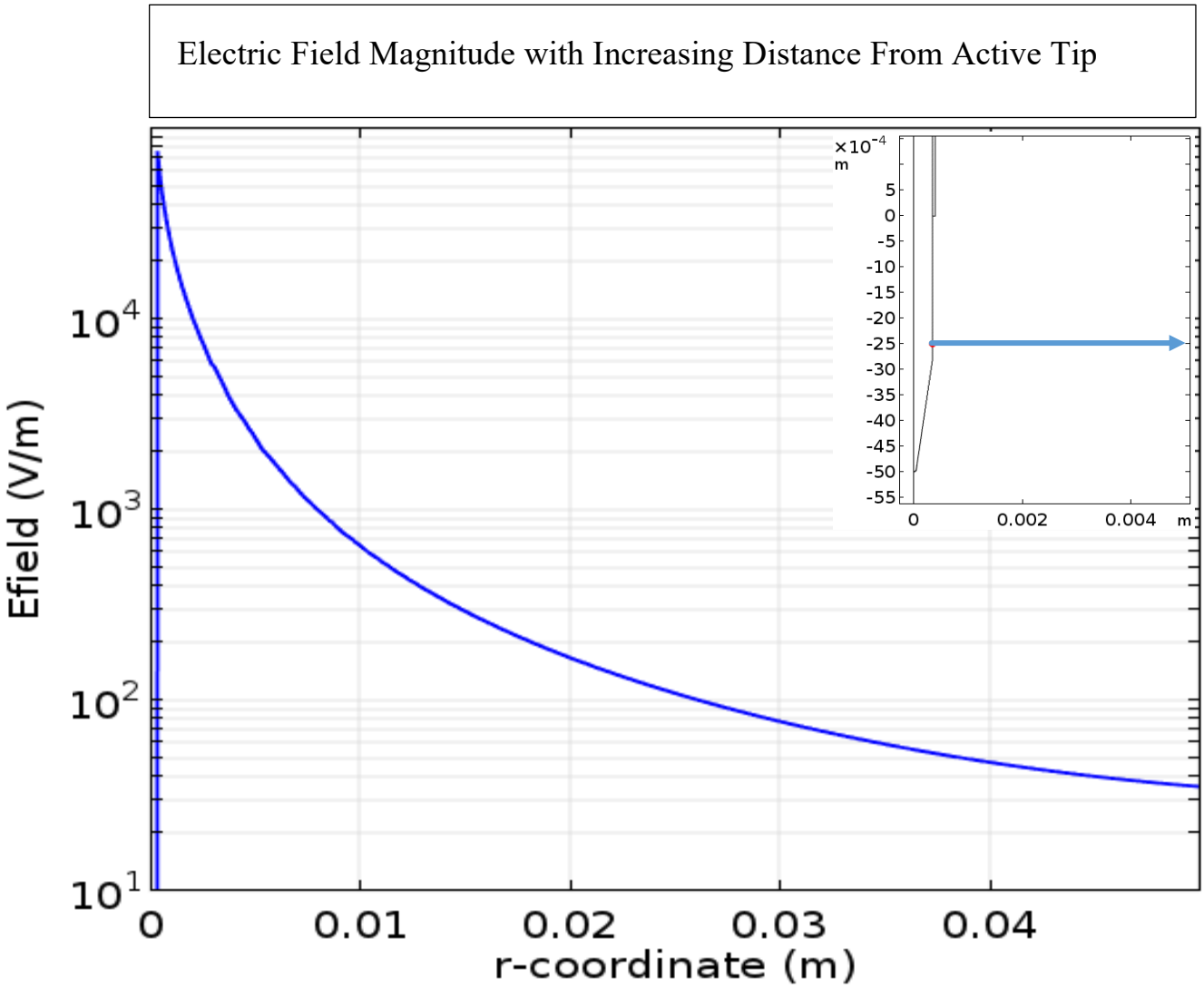

Figure 28 - Electric field magnitude drop off as radial distance increases. This sharp drop off makes it ideal for small targets.

Further quantitative comparison of electric field results can be seen in Figure 29 which shows temperature profile of Cosman and Cosman (2005) (left) and our simulation result (right) for both CRF and PRF mode with some electric field contour labels. It can be seen that in CRF mode with V_{rms} = 13 V, the temperature after 60 seconds reaches a higher value than it does in PRF mode with V_{max} = 70V. The figure also contrasts the electric field contour of the two modes to demonstrate how much stronger the electric field in PRF mode is. Differences between our results and those of Cosman and Cosman (2005) should also be noted. The 50 °C contour in CRF mode was not perfectly overlapped with the 2,500 V/m electric field contour as suggested in the result by Cosman and Cosman (2005). Also, in PRF mode we found some heating at the tip of the electrode which was not demonstrated by the results of Cosman and Cosman (2005). The electric field we found at the tip of the electrode was within 1.34% and 1.37% error for CRF and PRF mode respectively.

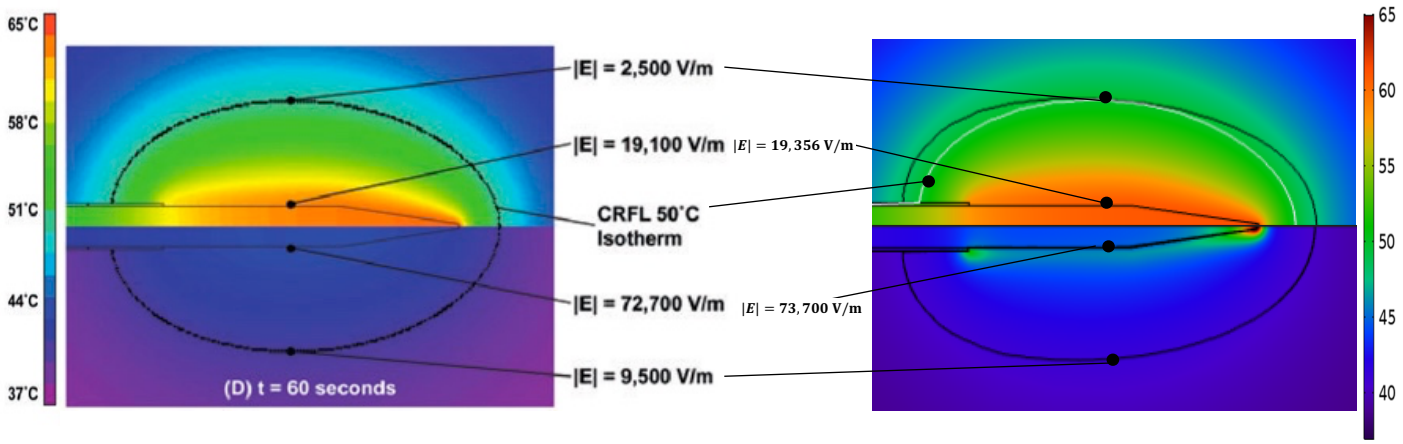

Figure 29 - On the left side, the heating result from Cosman and Cosman (2005) with CRF (top half) with the V_{rms}=13V and PRF (bottom half) with the V_{max}=70V after 60 seconds of treatment starting from 37°C. On the right side is our attempt to recreate their results with all of the same conditions. Cosman & Cosman labeled the 2,500 V/m electric field contour on the CRF model and 9,500 V/m on the PRF model.

3.3 Bipolar Simulation

To validate the simulation in the 3D bipolar mode, 3 CRF treatments and 2 PRF treatments were each carried out 3 times with the thermocouple placed between the RF probes. First, the pattern of the heating pattern was compared; in both experiment and simulation, the heating begins around the tip of the probe and the area between heats up as time goes on. The results in Figure 30 are solely for the visual inspection. This is because to take the image on the left, the treatment was conducted with the RF probes placed on the surface of the beef liver, rather than inserted into the tissue.

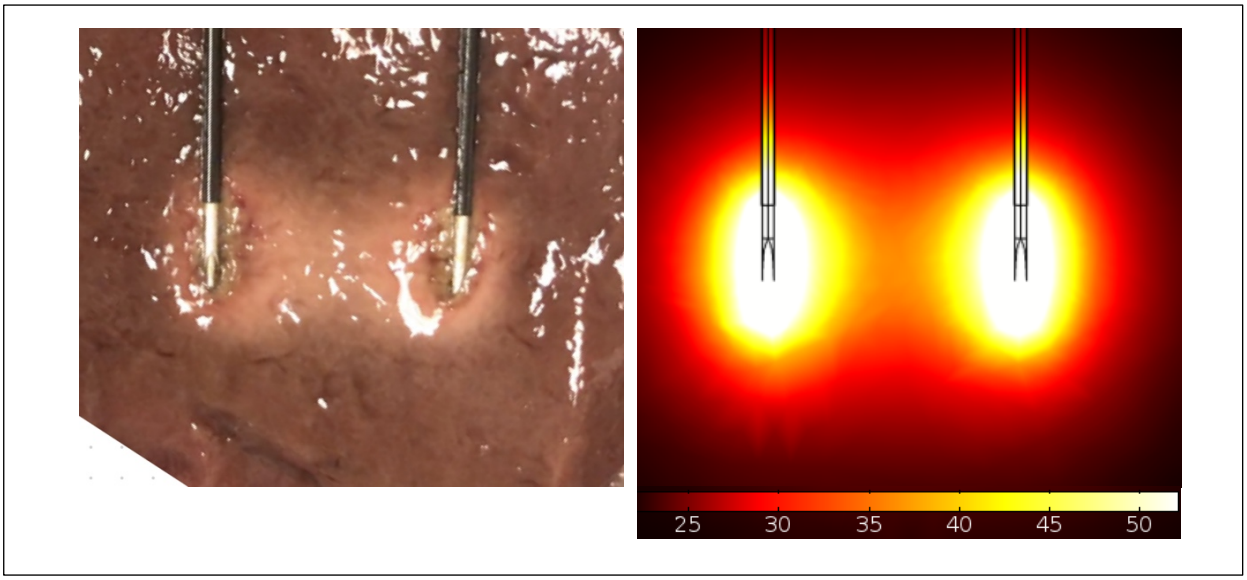

Figure 30 - An image of the bipolar RF lesion shape (left) and our model (right). The area closest to the probe experiences the most heating, and the effect spreads between the two probes.

The heating pattern can be visually validated with pictures and animations, but it was pertinent to validate the simulation quantitatively. This validation was done by producing the temperature profiles of comparing the simulation and experimental results and comparing them.

Figure 31 and Figure 32 outline the results from comparing our experimental and simulated results for both CRF and PRF treatments respectively.

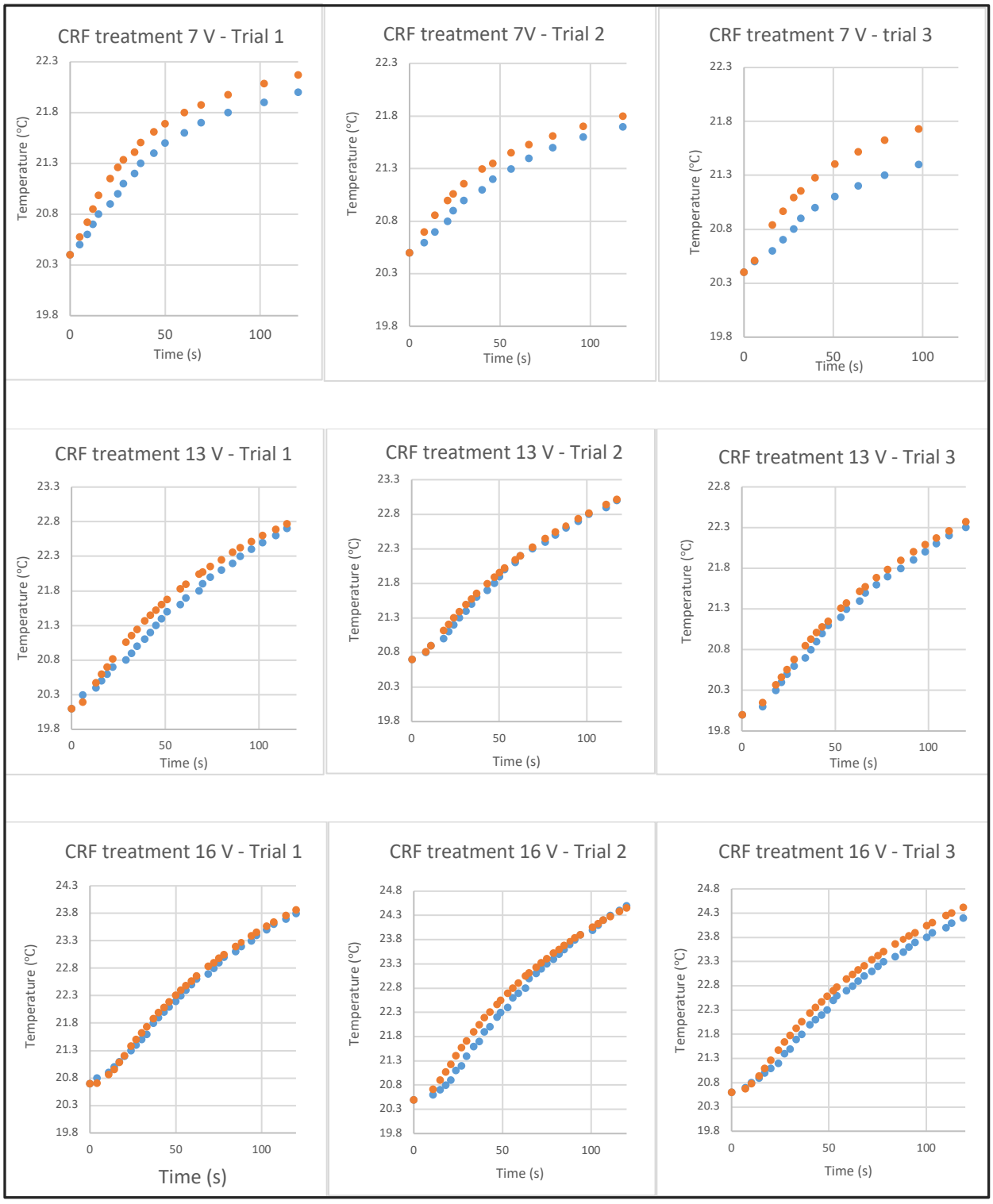

Figure 31 - The simulated (orange) and experimental (blue) results for 3 CRF treatment conditions. Each condition was carried out 3 times. Ramp time and initial temperature could have varied slightly for each trial but were accounted for in our simulation.

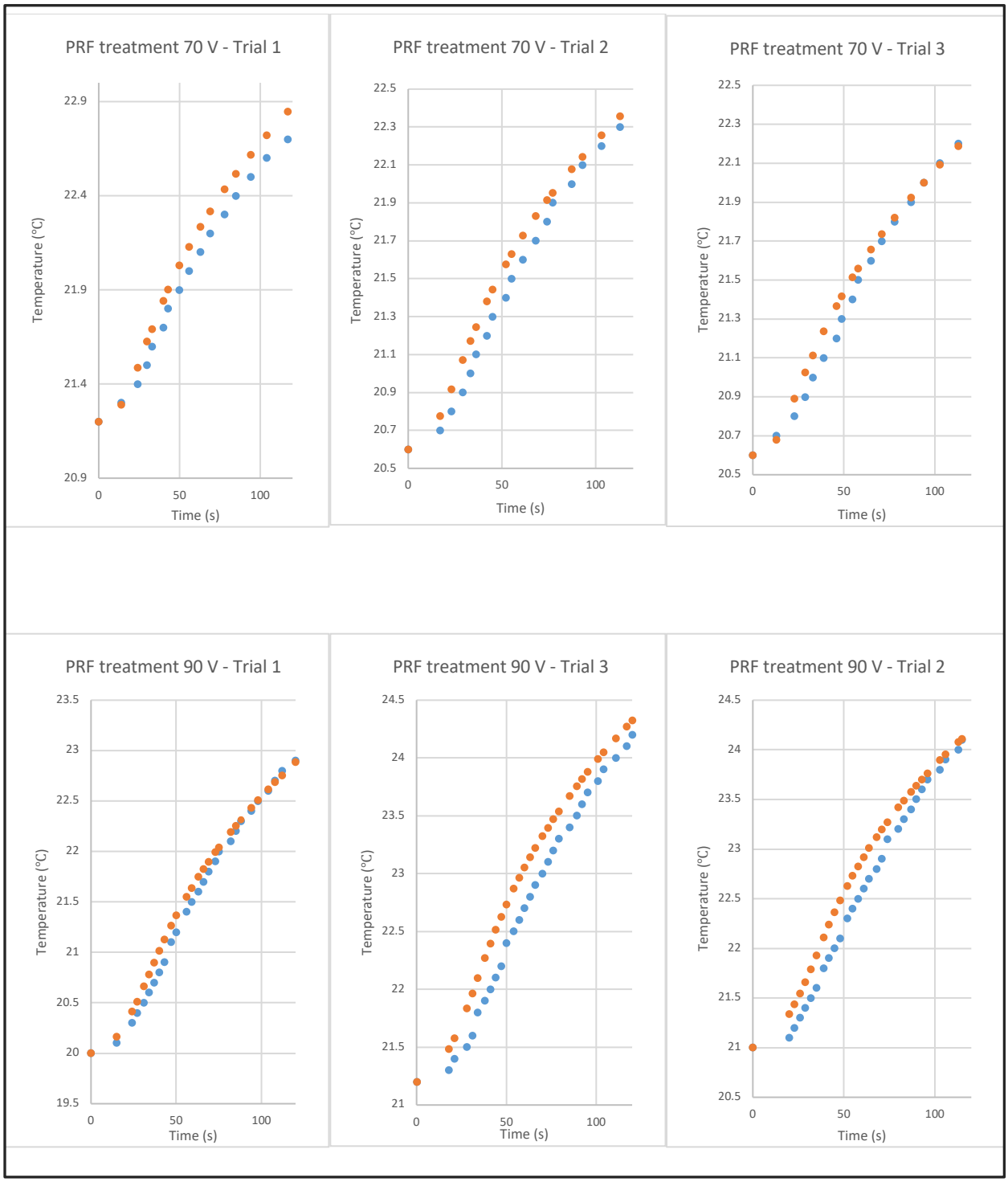

Figure 32 - The simulated (orange) and experimental (blue) results for 2 PRF treatment conditions. Each condition was carried out 3 times. Ramp time and initial temperature could have varied slightly for each trial but were accounted for in our simulation.

To analyze how precise the model was, the average absolute difference between the measured temperature and the simulated temperature was calculated. It was found that for all data

points ($n = 332$), the model predicted the temperature within ± 0.16 ℃. The average difference in temperature rise for all data points was 17.5 %. The breakdown by treatment condition can be seen in Table 3.

Table 3 - Evaluating the accuracy of our model vs experimental results

Voltage	n	Average Difference (C°)	Average Error (%)
CRF 7V	38	0.206	25.66
CRF 13V	70	0.110	10.96
CRF 16V	94	0.171	20.43
PRF 70V	48	0.107	14.80
PRF 90V	82	0.210	17.57
Total / Average	332	0.162	17.51

These experiments validated that the simulation was reliable and that further realistic simulations could be explored to investigate thermal effects.

3.4 Earthworm Simulation Results

The heating pattern seen in Figure 33 suggests that our electrode placement was suffice for treating the earthworm ventral nerve cord.

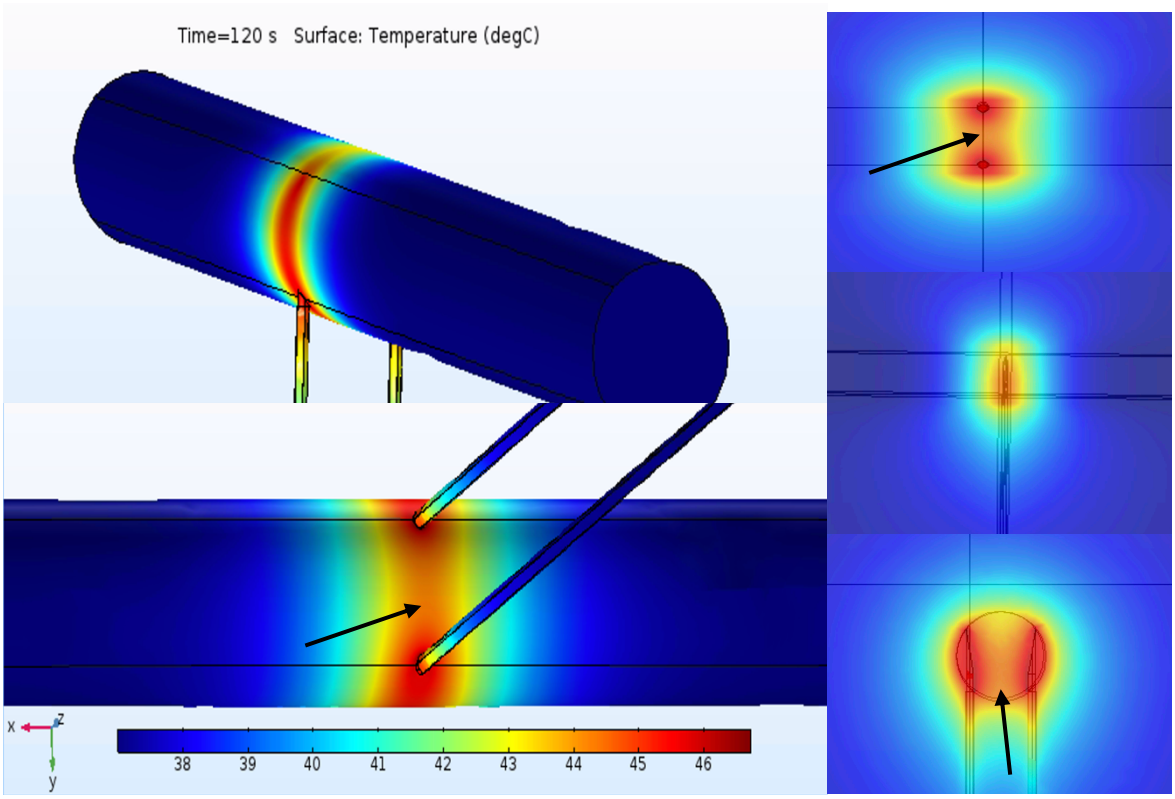

Figure 33 - Earthworm simulation heating pattern after 120 seconds of treatment with 70V PRF, 2 Hz pulse repetition rate, 20 ms pulse width. The snapshots on the left illustrate the heating of the surfaces. On the right are the three slices of the earthworm heating. The arrows indicate where the expected earthworm nerve would be and thus showing that the RF electrodes target the nerve accurately in this treatment set up.

It should be noted that the earthworm simulation model has two main limitations. The first limitation is that requisite earthworm material properties could not be found in literature and thus, in the current set up was modeled as a liver. The relatively high electrical conductance $\sigma = 0.29\ (\mathrm{S/m})$ of liver (for example compared to water where $\sigma = 10^{-10}\ (\mathrm{S/m})$) results in the overestimation of temperature. To simulate it as an earthworm, the material properties including

heat capacity, density, electrical conductivity, relative permittivity, and thermal conductivity need to be determined. The second limitation is with the thermal dose model. The thermal dose model requires the baseline temperature to be 37 ℃, and in our experiments, earthworms were treated at room temperature. One potential to rectify this situation would be to increase the starting temperature to 37 ℃ with a water bath and redo all of the experiments. Due to time constraints this was not attempted. Simulating from 37 ℃ as an initial starting point resulted in a final temperature of 44.4 ℃ or 1.2 CEM43℃ thermal dose to the earthworm-shaped liver tissue.

3.5 Vertebra Simulation

Figure 34 shows the heating of C6 vertebra for a PRF treatment of 120 seconds with 45V pulses of 20 ms pulse width at a rate of 2 Hz vertebra from three orientations. Heat is shown on the surface of the bone and RF electrodes, as well as slices of surrounding muscle. The vertebra simulation required a very dense mesh in order to avoid meshing errors, and thus took four days to simulate. We find that the positioning of the electrodes successfully targeted the medial branch since the most heating of the bone is found at the location of the medial branch. The target area where the

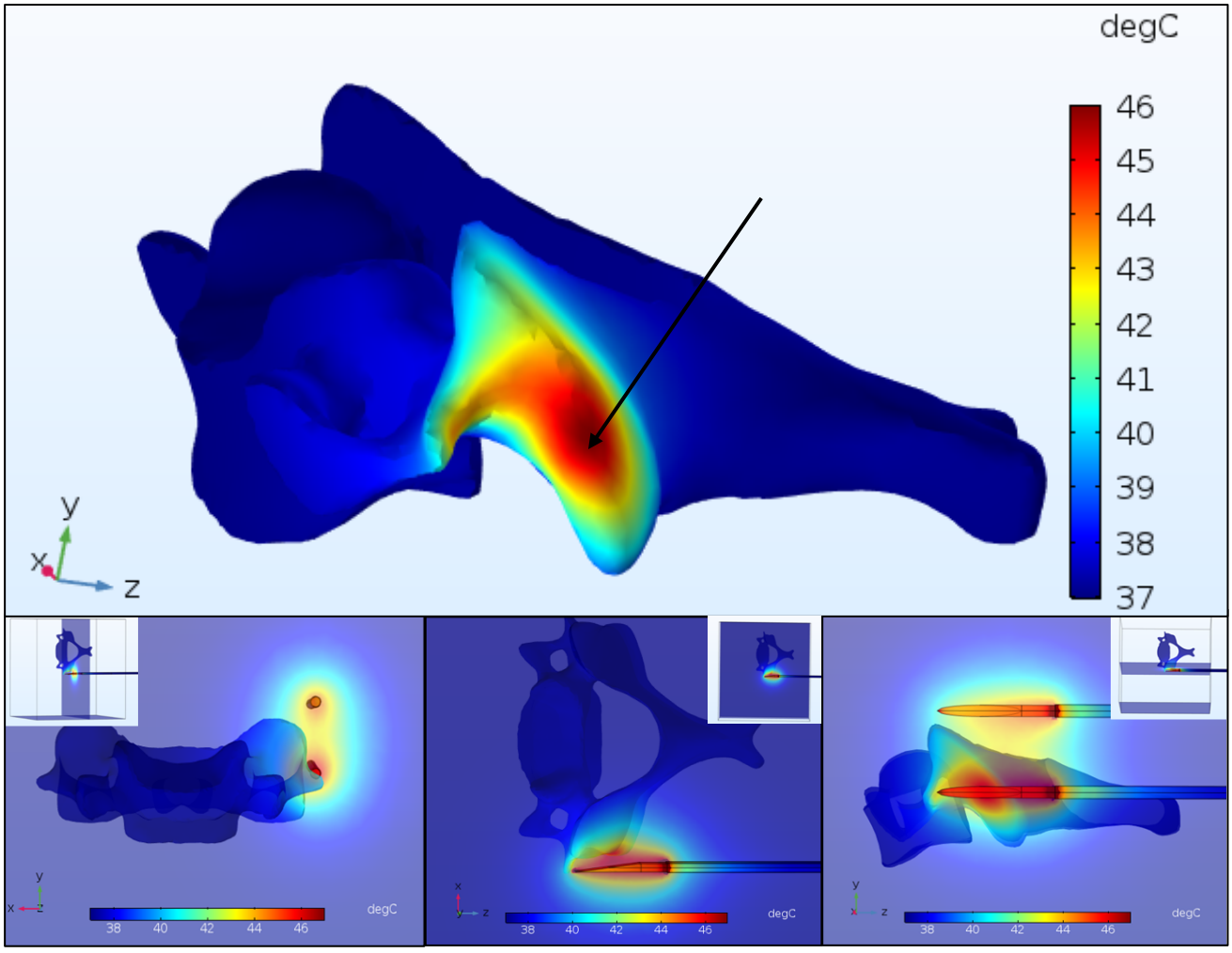

Figure 34 - Top image showing the surface of the C6 vertebra after 120 seconds PRF treatment. The hottest point was found at the location of the medial branch and used for thermal dose calculation. The image is accompanied by the smaller images below which are showing three slices as well. Note that the material surrounding the RF probes and C6 vertabra is assigned as muscle.

medial branch would appear shows a temperature of 46℃ after 120 seconds. The temperature profile can be seen in Figure 35 and was used to calculate the thermal dose to be 6.5 CEM43℃, which falls below the threshold of 10 CEM43℃. This would suggest that PRF effects are due to non-thermal effects, further supporting the hypothesis that the electric field exposure plays a major role.

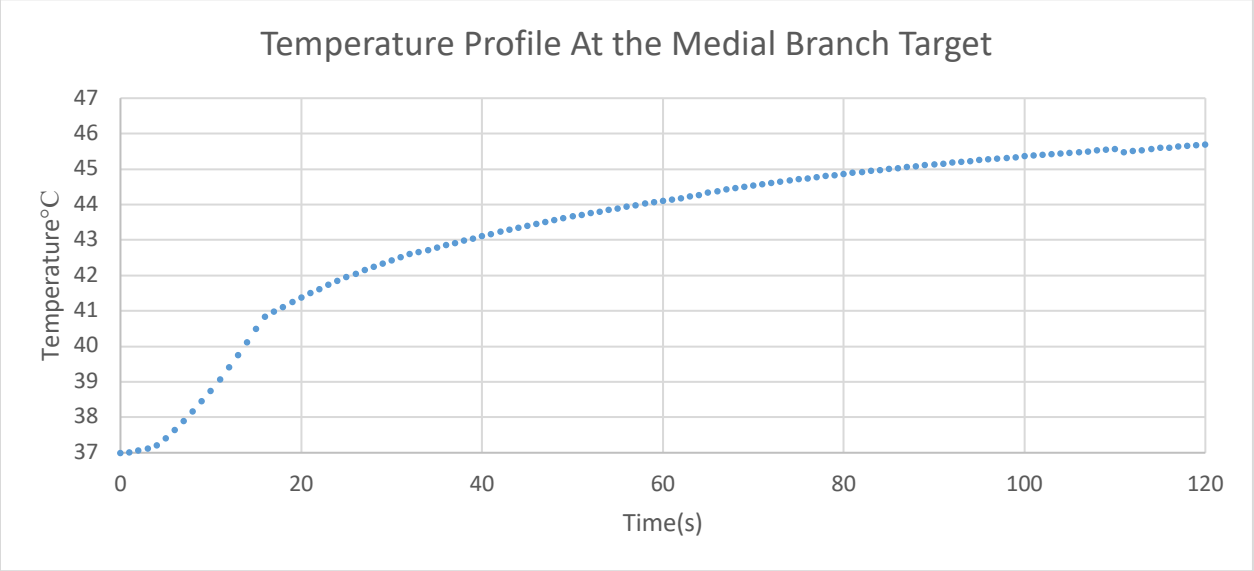

Figure 35 - Temperature profile at the location of the medial branch in the C6 PRF simulation.

By simulating the electromagnetics as a quasistatic model and only evaluating the temperature as a time-dependent study, we kept the simulation times at a reasonable time. The longest simulation was the vertebra simulation which took 4 days to simulate for a PRF mode treatment of 120 seconds. The PRF simulations always took longer to compute than CRF simulations. This is because in CRF mode, the solver can calculate with any time-steps that the user requires. For example, in this study time-steps of 1 second were suffice for a total of 120 time-steps. However, in PRF mode, the solver took 1 ms time-steps. To get to 120 seconds in PRF mode, the solver would make calculations for 120,000 time-steps.

4 Summary and Conclusion

In this study I found that bipolar PRF therapy was able to block the propagation of action potentials in earthworm nerves. With 90V pulses of 20 ms pulse width at a rate of 2 Hz, 6 out of 10 earthworms experienced a block of both nerves. There was no measurable change of temperature detected at the RF electrode tip, and the earthworms remained alive which was confirmed when observing movement in the head area after anesthesia had worn off.

I also created simulations capable of calculating the electromagnetics and bioheat physics of RF treatments. The model allows the user to select for monopolar or bipolar mode of current application, as well as continuous or pulsed. The user can select the desired pulse width, pulse repetition rate, peak voltage, ramp time and geometric settings with user inputs. After the simulation models were created, they were validated with the liver experiment. Temperature versus time readings with both CRF and PRF mode treatments were made and compared. Next, a realistic simulation was created with a C6 vertebra geometry surrounded by muscle tissue. Probes were placed to target the medial branch nerve. The temperature data at the targeted point were used to calculate the thermal dose at the location, which was determined to be 6.5 CEM43°C. This value is below the threshold of 10 CEM43°C for thermal damage.

The results indicate that in the field of chronic pain management, PRF acts on the target tissue in a non-thermal manner. In the future, studies should be carried out to investigate the effect of electric field exposure at a cellular level to structures found in axons (voltage gated channels, sodium potassium pump, etc).

Additionally, preliminary experiments were done to test the feasibility of conducting the PRF treatment simultaneously with the BIOPAC signal recording to find the exact point at which the earthworm nerve is blocked. Results are shown in Figure 36.

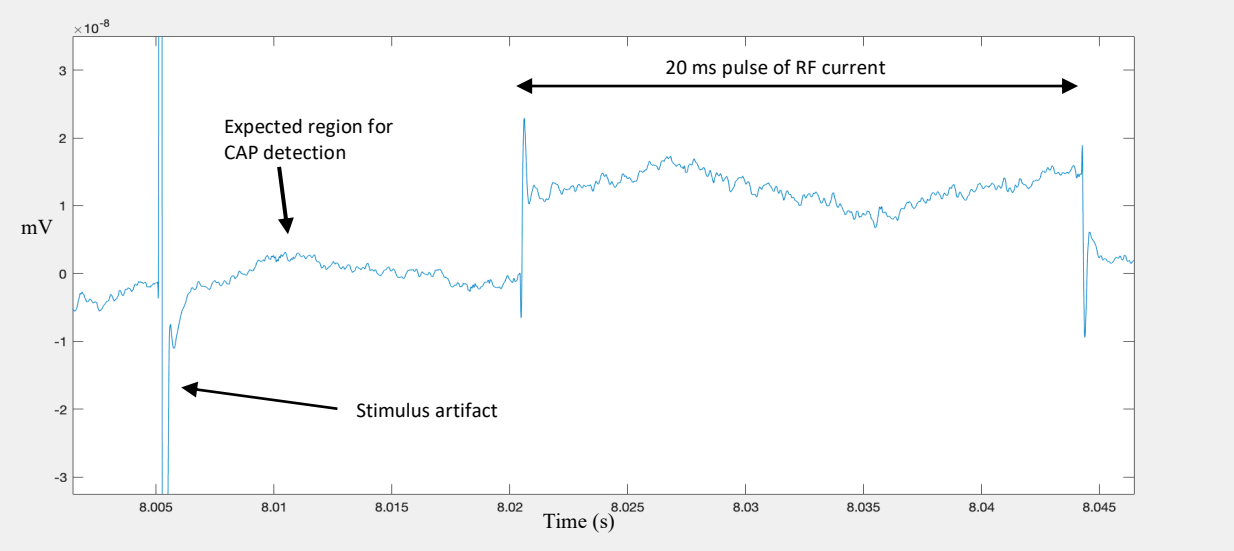

Figure 36 - BIOPAC response while the RF treatment takes place. In this particular case, there is no nerve response recorded

It was decided that this experimental set-up could damage the sensitive BIOPAC reading electrodes and thus was not pursued. If this set-up could be made viable and the earthworm material properties could be found, hypothetically a value for electrical field exposure could be found at which nerves are no longer able to propagate action potential. This would allow clinicians in the future to optimize PRF set-up in the treatment to improve the outcomes of chronic pain management.

Appendix A – COMSOL Pulse and Ramp Function

An adjustment had to be to the CRF model to accommodate for pulsed RF. For PRF modeling, I decided to pulse the heating source in bioheat transfer in order to keep the electromagnetics study stationary as it was initially. This was to avoid implementing two time-dependent studies in the same simulation. Figure A1 demonstrates an analytic global function used to create the pulse with the following parameters

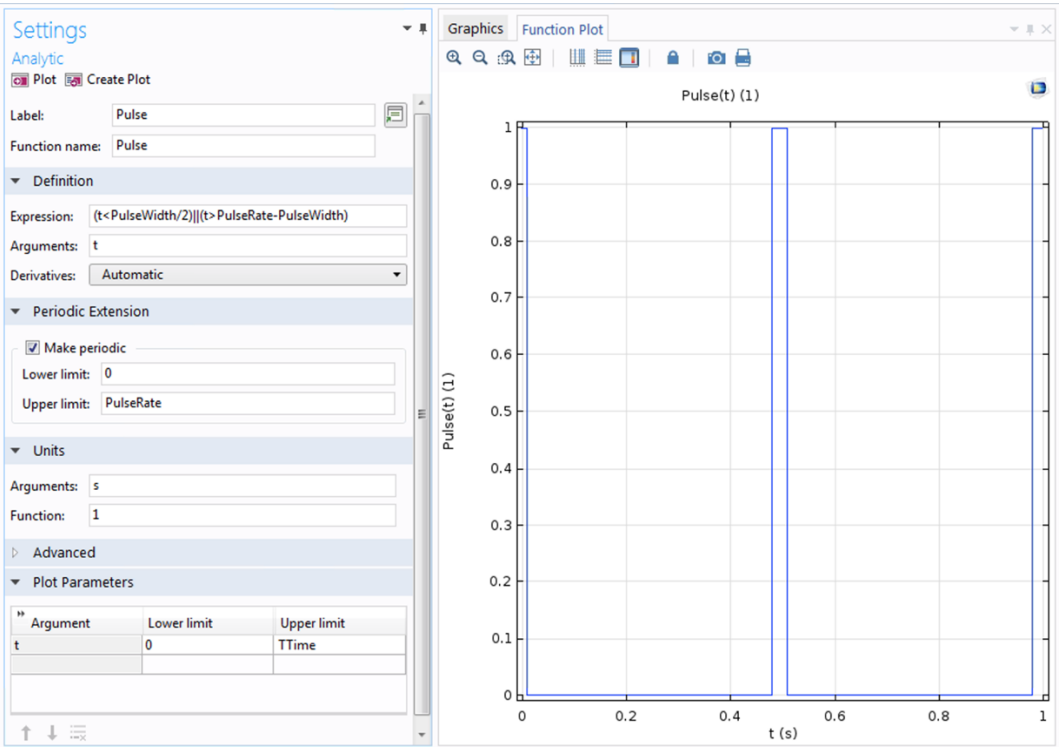

Figure A1 - COMSOL interface for analytical function to create a pulsing function

where *PulseWidth, PulseRate* (which is actually period of the on/off cycle), and *TTime* (treatment time) are global parameter that can easily be adjusted. In the example above, the *PulseWidth* is set to 20 ms, *PulseRate* is set to 0.5 seconds (2 Hz Pulse rate), and *TTime* is set to 1 second for easier visualization. The new Pulse(t) function is multiplied by the heat source, which was previously given the variable name *PDense*.

In order for the solver to accommodate the pulsing function, one more component was added to the model. This was done by clicking *add physics*, opening the *mathematics* menu, *ODE and DAE interfaces,* and selecting *Events (ev)*. In the Model Builder, two *explicit events* were added and set up as shown in Figure A2.

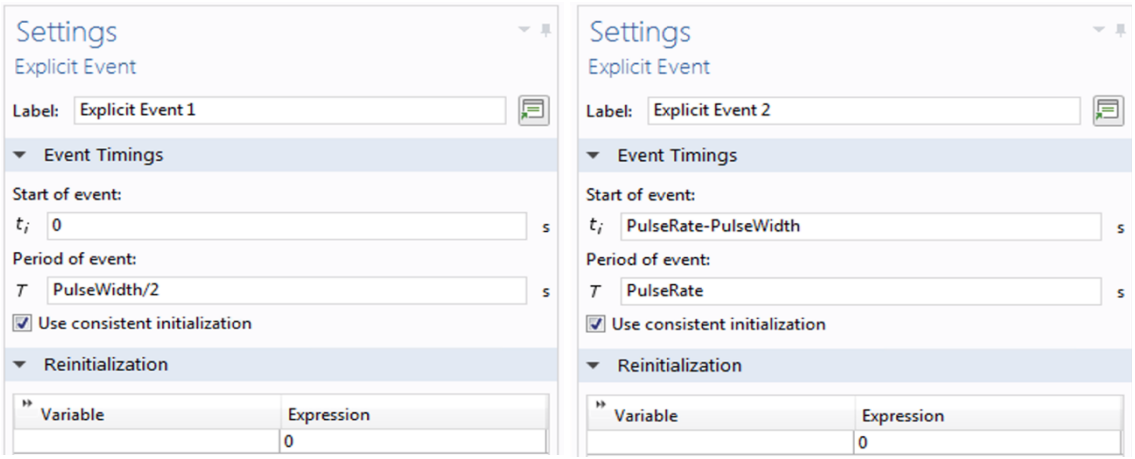

Figure A2 - Settings for explicit events required for the solver to adequately accommodate the pulsing function. Two explicit events are required, one for 'on' and one for 'off'.

Finally, to run the simulation, one study was created with two steps. The first step (stationary) computed the electric field (only electrostatics *(es)* is selected, bioheat *(ht)* and events *(ev)* are not), and the second step (time-dependent) solved for heat distribution with respect to time (bioheat *(ht)* and events (*ev)* are selected, electrostatics *(es)* is not).

In practice, RF generators ramp up the current from 0. This can take up to 30 seconds. In order to create a simulation that was as realistic as possible, a ramp function was also created (Figure 39) which was multiplied by the pulse function to create a final function that both pulses, and ramps. To create the ramp function another global analytic function is added and set up as shown below. The example below has a ramp time of 5 seconds, and a treatment time (*TTime*) of 20 seconds.

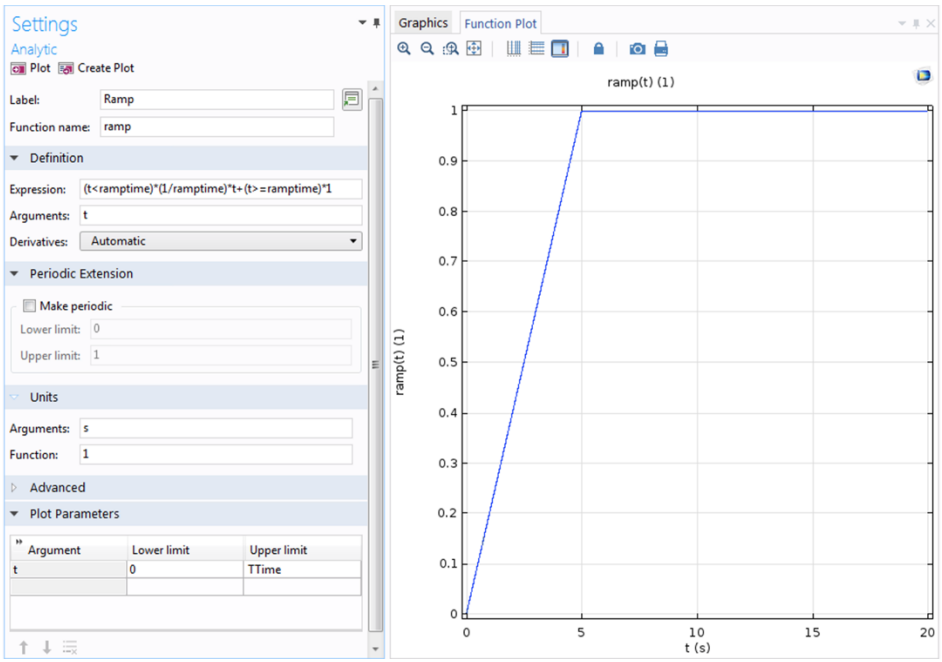

Figure A3 - In realistic RF applications, there is a ramping period. This analytical function allows the voltage to be ramped up.

The ramp function and the pulse function can be multiplied together by creating another global analytical function and an example of the result can be seen below in Figure A4.

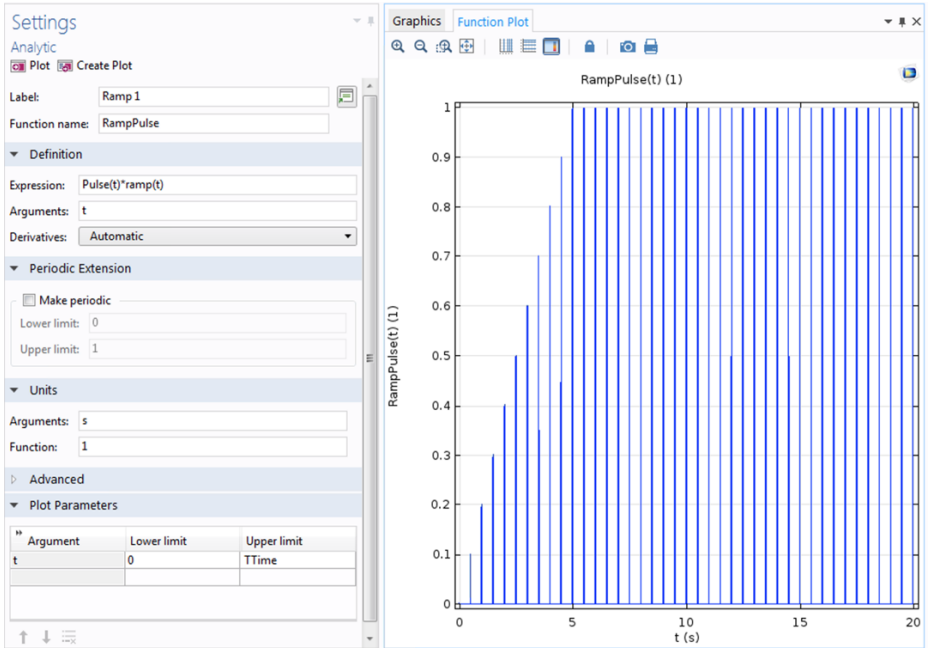

Figure A4 - The result of the pulsing function multiplied by the ramping function. This function is then multiplied by the heating source.

Bibliography

1. Basser DS. Chronic pain: A neuroscientific understanding. *Med Hypotheses*. 2012;78(1):79-85.

2. Loeser JD. What is chronic pain? *Theor Med*. 1991;12(3):213-225.

3. Wong A. Government of Canada — Action for Seniors report. Government of Canada. https://www.canada.ca/en/employment-social-development/programs/seniors-action-report.html. Published 2014

4. Lynch ME. The need for a Canadian pain strategy. *Pain Res Manag*. 2011;16(2):77-80.

5. Breivik H, Collett B, Ventafridda V, Cohen R, Gallacher D. Survey of chronic pain in Europe: Prevalence, impact on daily life, and treatment. *Eur J Pain*. 2006;10(4):287-333.

6. Schopflocher D, Taenzer P, Jovey R. The Prevalence of Chronic Pain in Canada. *Pain Res Manag*. 2011;16(6):445-450.

7. Darnall BD. *Psychological Treatment for Patients with Chronic Pain.*; 2019.

8. Gomes T, Khuu W, Martins D, et al. Contributions of prescribed and non-prescribed opioids to opioid related deaths: Population based cohort study in Ontario, Canada. *BMJ*. 2018;362.

9. Fitch P. The Canadian Opioid Crisis: CSHP's Commitment. *Can J Hosp Pharm*. 2018;71(3):2018.

10. Frey G (Reuters). Purdue Pharma files for bankruptcy to wipe out 2,000 OxyContin lawsuits. *Financial Post*. https://business.financialpost.com/news/fp-street/oxycontin-maker-purdue-pharma-files-for-bankruptcy-to-wipe-out-2000-lawuits. Published September 16, 2019.

11. Serpell M, Ratcliffe S, Hovorka J, et al. A double-blind, randomized, placebo-controlled, parallel group study of THC/CBD spray in peripheral neuropathic pain treatment. *Eur J Pain (United Kingdom)*. 2014;18(7):999-1012.

12. Scott A, Guo B. *Trigger Point Injections For Chronic Non-Malignant Musculoskeletal PAin*. Edmonton, Alberta: Alberta Heritage Foundation for MEdical Research; 2005.

13. Vigneri S, Sindaco G, La Grua M, et al. Combined epidural morphine and bupivacaine in the treatment of lumbosacral radicular neuropathic pain: A noncontrolled prospective study. *J Pain Res*. 2016;9:1081-1087.

14. Bard H, Marty M, Rozenberg S, Laredo JD. Epidural corticosteroid injections: Still credible? *Jt Bone Spine*. 2019;86:531-534.

15. Najafi A, Sartoretti E, Binkert CA. Sacroiliac Joint Ablation Using MR-HIFU. *Cardiovasc Intervent Radiol*. 2019;42(9):1363-1365.

16. Lu K, Liliang PC, Liang CL, Wang KW, Tsai YD, Chen HJ. Efficacy of conventional and pulsed radiofrequency for treating chronic lumbar facet joint pain. *Formos J Surg*. 2012;45(4):107-112.

17. VanPutte C, Regan J, Russo A, Seeley R. *Seeley's Anatomy & Physiology*. 10th ed. New York: McGraw-Hill; 2014.

18. Voscopoulos C, Lema M. When does acute pain become chronic ? *Br J Anaesth*. 2010;105:69-85.

19. Xu K, Terakawa S. Chapter 10 - Three Mechanisms or Strategies for Increasing Conduction Velocity of Nerve Fibers. In: *Myelinated Fibers and Saltatory Conduction in the Shrimp*. Springer, Tokyo; 2013:83-90.

20. Metso AJ, Palmu K, Partanen J V. Compound nerve conduction velocity - A reflection of proprioceptive afferents? *Clin Neurophysiol*. 2008;119(1):29-32.

21. Feizerfan A, Sheh G. Transition from acute to chronic pain. *Contin Educ Anaesthesia, Crit Care Pain*. 2015;15:98-102.

22. Sapareto SA, Dewey WC. Thermal Dose Determination in Cancer Therapy. *Int J Radiat Oncol Biol Phys*. 1984;10(February):787-800.

23. Van Rhoon GC, Samaras T, Yarmolenko PS, Dewhirst MW, Neufeld E, Kuster N. CEM43°C thermal dose thresholds: A potential guide for magnetic resonance radiofrequency exposure levels? *Eur Radiol*. 2013;23(8):2215-2227.

24. Monafo WW, Eliasson SG. Sciatic nerve function following hindlimb thermal injury. *J Surg Res*. 1987;43(4):344-350.

25. Soloman M, Mekhail MN, Mekhail N. Radiofrequency treatment in chronic pain. *Expert Rev Neurother*. 2010;10(3):469-474.

26. Byrd D, Mackey S. Pulsed Radiofrequency for Chronic Pain. *Curr Pain Headache Rep*. 2008;12:37-41.

27. Rea W, Kapur S, Mutagi H. Radiofrequency therapies in chronic pain. *Contin Educ Anaesthesia, Crit Care Pain*. 2011;11(2):35-38.

28. Chua NHL, Vissers KC, Sluijter ME. Pulsed radiofrequency treatment in interventional pain management: Mechanisms and potential indications - A review. *Acta Neurochir (Wien)*. 2011;153(4):763-771.

29. Hanakawa T. Neural mechanisms underlying deafferentation pain: A hypothesis from a neuroimaging perspective. *J Orthop Sci*. 2012;17(3):331-335.

30. Ewertowska E, Mercadal B, Muñoz V, Ivorra A, Trujillo M, Berjano E. Effect of applied voltage, duration and repetition frequency of RF pulses for pain relief on temperature spikes and electrical field: a computer modelling study. *Int J Hyperth*. 2018;34(1):1-10.

31. Erdine S, Bilir A, Cosman Sr ER, Cosman Jr ER. Ultrastructural Changes in Axons Following Exposure to Pulsed Radiofrequency Fields. *Pain Pract*. 2009;9(6):407-417

32. Cosman ER. Electric and Thermal Field Effects in Tissue Around Radiofrequency Electrodes. *Pain Med*. 2005;6(6).

33. Cosman ER. A Comment on the History of the Pulsed Radiofrequency Technique for Pain Therapy. *Anesthesiology*. 2005;103(6):1311-1321.

34. Habash R. *Bioeffects and Therapeutic Applications of Electromagnetic Energy*. CRC Press; 2007.

35. Kladt N, Hanslik U, Heinzel H. Teaching Basic Neurophysiology Using Intact Earthworms. *J Undergrad Neurosci Educ*. 2010;9(1):20-35.

36. Shannon KM, Gage GJ, Jankovic A, Wilson WJ, Marzullo TC. Portable conduction velocity

experiments using earthworms for the college and high school neuroscience teaching laboratory. *Adv Physiol Educ*. 2014;38(1):62-70.

37. Haus HA, Melcher JR. Electromagnetic Fields and Energy - Chapter 3: Introduction to Electroquasistatics and Magnetoquasistatics. In: *Electromagnetic Fields and Energy*. Prentice-Hall; 2008. http://ocw.mit.edu/.

38. Hashemi M, Hashemian M. Effect of pulsed radiofrequency in treatment of facet-joint origin back pain in patients with degenerative spondylolisthesis. *Eur Spine J*. 2014;23:1927-1932.

39. Frei W. Study Radiofrequency Tissue Ablation Using Simulation. COMSOL Multiphysics.